

1

Introduction to Supported Metal Single Atom Catalysis

Doan Pham Minh¹ and Philippe Serp²

¹Université de Toulouse, IMT Mines Albi, UMR CNRS 5302, Centre RAPSODEE, Campus Jarlard, F-81013, Albi Cedex 09, France

²Université de Toulouse, LCC, CNRS-UPR 8241, ENSIACET, 31030 Toulouse, France

1.1 Introduction

Supported metal catalysts are extensively used in the chemical industry, from bulk and fine chemicals production to petrochemicals. In this family of catalysts, the support contributes to maintain a high dispersion of the active phase, improves catalyst stability (including mechanical) but also determines at a certain extent the physico-chemical properties of the active phase, and thus its activity. When considering most of this support effects, the size of metal particles is an important parameter to consider. For large particles (10–100 nm), the influence of the support will be limited to the interface (interfacial effects), and will involve a limited number of metallic atoms, and the support effect can be diluted by the presence of the numerous metal atoms located far away from the support. The interfacial effects between the support and catalyst could control electron distribution, tune intermediate adsorption, prevent catalysts from dense aggregation, and improve stability. Thus, if we consider charge transfer, which can have a substantial influence on adsorption and, therefore, on reactivity, it can be expected that for large particles the average number of electron transfer per metal atom will be smaller than for small particles [1]. It is however important to note that due to strong charge screening, the excess of charge on metal particle could be expected to accumulate at the direct contact interface (sub-nanometer short-range charge transfer) [2]. Interfacial sites can also contribute to tune intermediate adsorption. For example, in the Sabatier reaction, an enhanced cooperation between nickel and interfacial active sites was reported [3, 4], which leads to rapid dissociative adsorption of H₂ on Ni and hydrogen spillover. The H atoms generated contribute to CO₂ hydrogenation and create oxygen vacancies on the reducible support surface, which contribute to CO₂ adsorption and activation. In that context, it is interesting to decrease the particle size. As particle size decreases (1–10 nm), these interfacial effects will be exacerbated, but other phenomena should be taken into consideration, such as the increase in surface defects (uncoordinated metal atoms) and even quantum size effects in the case of very small

particles (clusters), which can of course dictate the catalytic activity [5, 6]. In the latter case, although tremendous variation in the relationships between size and activity exist depending on the system studied, these relationships are often broken into: positive size-sensitivity reactions, negative size-sensitivity reactions, size-insensitive reactions, and a fourth category composed of reactions for which a local minima or maxima in activity exists at a given particle size [7, 8]. Going back to the Sabatier reaction, structure sensitivity over nickel catalysts was reported in the 1–7 nm range, with a maximum in activity at 2.5 nm [9]. The smallest Ni particles bind CO too weakly, facilitating its easy desorption and modifying the selectivity of the reaction.

Downsizing metal catalyst particles to supported metal single atoms is the ultimate step. In that case, some interfacial effects can be exacerbated like the electronic metal-support interactions and other intrinsic metal effects, such as the electronic quantum size effect and the structure-sensitivity geometrical effect disappear. We thus arrive at a situation where the role of the support, which one has to see as a ligand as in homogeneous or enzymatic catalysis, becomes preponderant. Indeed, it will have a direct influence on the charge state, oxidation state and structure of the frontier orbitals of the active site, which is now limited to an isolated metal single atom (Figure 1.1). Furthermore, in this case, tuning of the support surface chemistry can even be as relevant as the selection of the supported metal itself for regulating the catalytic activity [10].

Of course, such a size reduction raises questions other than chemical reactivity. How to produce such species and how to characterize them reliably? The progress made since the beginning of this century in terms of synthesis, characterization and modeling strategy has made it possible to see the emergence of a new class of catalysts: metal-supported single-atom catalysts (SACs). The catalysis community

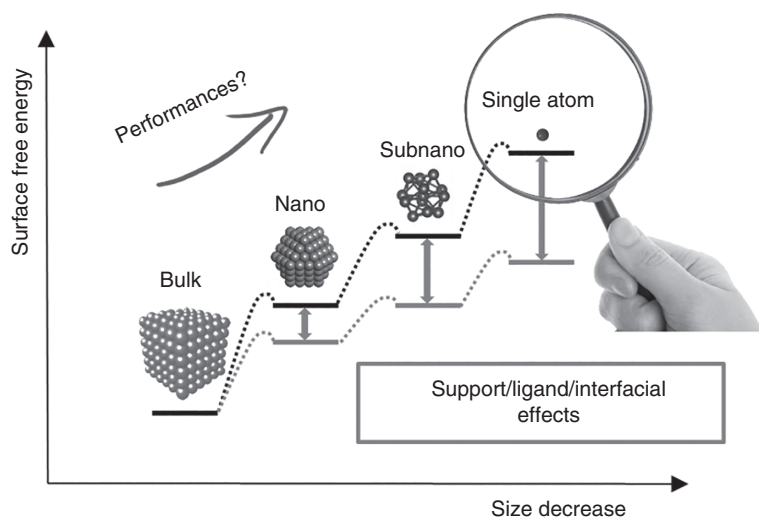


Figure 1.1 Influence of downsizing of catalyst particles on interfacial effects. Source: Philippe Serp.

quickly recognized the importance of metal supported single atom catalysis [11–17], which can be seen as the ultimate consequence of applying the atom economy concept to heterogeneous catalysis. The First International Symposium on Single-Atom Catalysis (ISSAC) was organized in 2016 by T. Zhang, J. Li, and J. Liu at Dalian Institute of Chemical Physics in Dalian, China, in 2016. Since then, an exponential number of publications, including review articles and patents on that subject are published every year.

Supported metal single atom catalysis has often been presented as a bridge between heterogeneous and homogeneous catalysis [17–19]. On one side (where we mainly find the heterogeneous catalysis community), it is true since at the active site, a single metallic atom is surrounded by a ligand (the support) just like in homogeneous system. On the other side (where most molecular chemists stand), a difference exists linked to the presence of a surface that plays the role of a solid, “rigid” ligand with specific redox, acid-base, as well as physical properties (e.g. porosity, hydrophilicity, hydrophobicity, semiconducting properties, etc.). We will also notice that the diversity of direct environment in supported metal SACs, i.e. the first coordination sphere is rather limited compared to homogeneous systems. Indeed, on oxide, it is often limited to a metal-O environment, and on carbon metal-C, metal-N₄ (like in metalloporphyrine) metal-O or metal-S bondings have been regularly reported. Additionally, for oxide supports, beyond the first coordination sphere (O-coordination), metal cations on oxide supports readily serve as the second coordination sphere and are involved in catalytic reactions together with the primary catalytic metal single atoms [20]. The presence of such “macromolecular” ligands can induce specific properties to the metal and *in fine* to the resulting supported catalysts that most of the homogeneous systems do not present [16]. Most, but not all... Thus, Jørgensen introduced the term “non-innocent” ligand in 1966 [21]. He stated “*ligands are innocent when they allow oxidation states of the central atom to be defined,*” which correspond to non redox-active ligands [22]. We will see in Section 1.4.3.2 of this chapter that the support can indeed, in some cases, behave as a “non-innocent” ligand and introduce complexity in the system. Additionally, in metal–ligand cooperative catalysis [23], ligands are involved (like in enzyme catalysis [catalytic residues] and in supported metal SACs [24] as we have seen for the Sabatier reaction) in facilitating reaction pathways that would be less favorable to occur solely at the metal center. Also, plastic deformation (a dynamic phenomenon) of the catalytic system can induce difference in reactivity as observed in heterogeneous catalysts [25–27], supported metal SAC [28], and enzymatic catalysis (allosteric sites) [29, 30].

From these various considerations, it appears that a number of factors must be carefully taken into account when trying to make correlation between the structure of supported metal SACs and their catalytic performances (Figure 1.2). Such a level of complexity positions supported metal single atom catalysis closer to enzymatic [31] or supramolecular catalysis [32] than to conventional homogeneous catalysis.

Finally, if metal-support interaction is certainly important for regulating catalytic performance of SACs, other type of cooperativity that are not specific to SACs, such as metal–ligand or heterobimetallic cooperativity, and cooperativity that

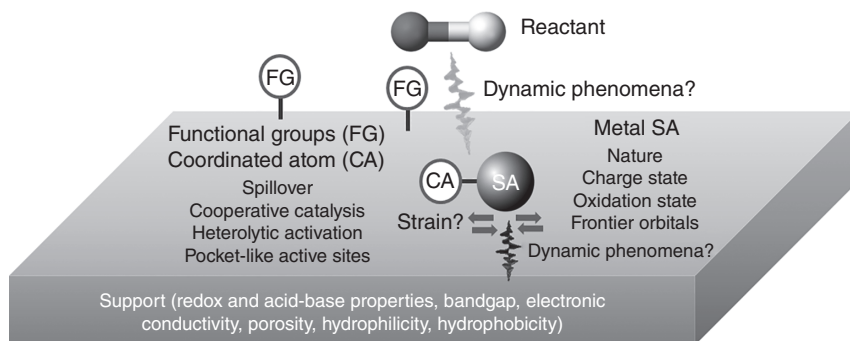


Figure 1.2 Factors affecting catalytic performances of supported metal SAC. Source: Philippe Serp.

are SAC-specific such as nanoparticle-single atom or mixed-valence single atom cooperativity have been reported [33].

1.2 Definition

One discussing about supported metal single atom catalysis, a first question is often asked *how different is tethered homogeneous catalysts or single-site heterogeneous catalysts (SSHCs) to supported metal single atom catalysts (SACs)?* To answer this question, we will rely on some definitions introduced by Thomas et al. [34], Basset and coworkers [16], and Liu [35].

For Thomas et al., an SSHC (catalytically active center) may consist of one (or more in the case of small clusters) atoms spatially isolated from one another. Each single site presents the same energy of interaction between it and a reactant; and is structurally well-characterized as for single site homogeneous molecular catalysts (Figure 1.3a) [34]. SSHCs may be conveniently classified into three main categories: (i) individual isolated ions, atoms, molecular complexes or well-defined clusters anchored to high-area supports; (ii) “ship-in-bottle” structures, in which isolated catalytic molecular entities are entrapped within a zeolite cage; and (iii) solid frameworks that host the catalytically active centers, zeolitic [36], and metal-organic frameworks (MOFs) [37] materials occupying an outstanding position since they are crystalline.

As far as tethered homogeneous catalysts are concerned, Basset distinguishes surface organometallic catalysts (SOMCats) that are directly bound to the surface, and where the surface acts as rigid ligand, and supported homogeneous catalysts (SHCs) where the metal atom is tethered to the support surface via flexible linkers coordinating the metal via covalent or noncovalent interactions (Figure 1.3b) [16]. In SOMCats and SHCs, the catalytically active sites are formed by reacting organometallic or coordination compounds with (functionalized) surfaces (oxides, metal nanoparticles, carbon). For these catalysts, the supported organometallic/coordination species keep at least part of their ligands after grafting. These types of catalysts can be classified as SSHCs if all of the active sites are structurally identical. This of course will

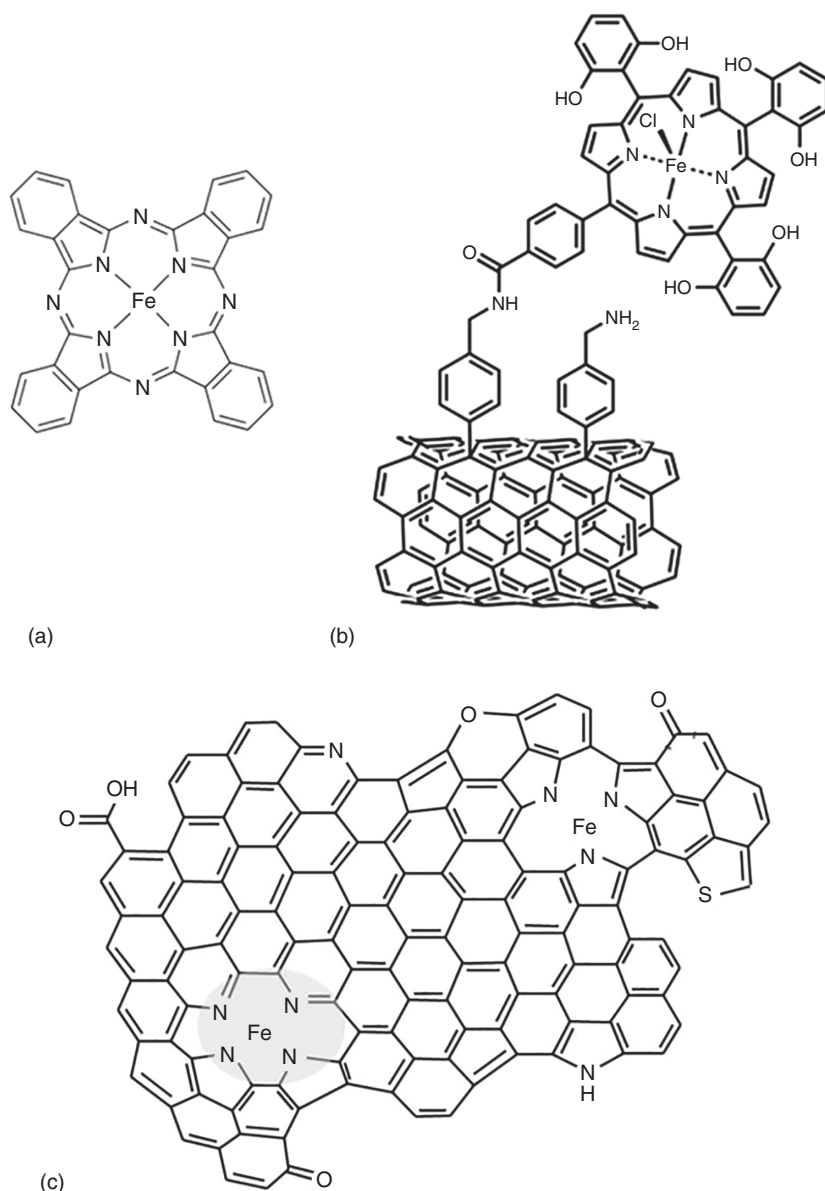


Figure 1.3 (a) A single site homogeneous molecular catalysts (iron(II) phthalocyanine complex); (b) a supported homogeneous catalysts (SHCs); and (c) a supported metal single atom catalyst. Source: Philippe Serp.

depend on the nature of the support. Indeed, if the supporting solid exposes different anchoring situations, the structure of the anchored sites is usually not well known.

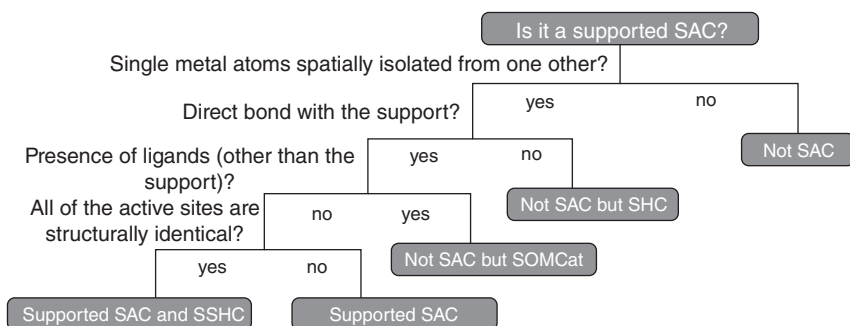
In supported metal SACs, only single metal atoms are present, which are dispersed on a solid support (Figure 1.3c) [35]. The interaction between the single atoms (SAs)

and the support can be of a different nature involving covalent, coordination, or ionic bonds. There should be no appreciable interactions among the isolated SAs.

The difference between SACs and SOMCats therefore lies in the presence of ligands on the metal generally originating from the precursor used during the synthesis. Of course, if these ligands are removed the SOMCat will transform into SAC. Likewise, if a supported SAC is modified by the addition of a ligand, it can be considered as a SOMCat. The active sites in SACs generally consist of the SAs, but in some cases the immediate neighboring atoms of the support surface can be involved. The catalytic property of the individual active sites can be similar or different depending on the interaction between the SA and its neighboring atoms of the support. When the catalytic behavior of all the metal SAs in a supported SAC is the same, then the SAC can be considered to be an SSHC as well (Scheme 1.1). This should not be the case of the SAC shown in Figure 1.3c, since the two Fe centers do not present the same environment. For supported double and triple metal atom catalysts discussed in *Chapter 15*, the same reasoning can be followed. Supported single, double, triple metal atom catalysts can be considered as a subset of atomically dispersed supported metal catalysts (ADSMCs) [35], together with two-dimensional rafts or very small clusters.

Following these definitions, there is no substantial difference between homogeneous and heterogeneous single-site catalysts since the ligand sphere around the metal, which is accurately engineered, should be the same in both cases. Additionally, supported SACs, SHCs or SOMCats can be considered as SSHCs if all of their active sites are structurally identical (Scheme 1.1), which is not often the case due to support inhomogeneity in term of anchoring sites.

It is worth noting that when considering supported SACs, the rules of molecular chemistry apply, and help to rationalize the structure and the reactivity of these species. This leads us to mention a point that seems important to us in this type of catalysis. If definitions are necessary to clarify the differences between all these types of catalysts, they should not make us forget the similarities. As we have seen, the SSHC family is very large and includes grafted molecular species and crystalline solids, which are generally studied by different communities (molecular chemists and materials chemists). Similarly, the objects involved in catalysis are



Scheme 1.1 Guide to the definition of supported single metal atom catalysts. Source: Philippe Serp.

often studied in different ways. Studies carried out on the most molecular catalysts (SHCs, SOMCats) are often mechanistic; while those relating to catalytic solids often also integrate traditional problems of heterogeneous catalysis and associated processes (transfer, diffusion, etc.). Interestingly, supported SACs lie in between grafted molecular species and crystalline solids and their study should be performed by multidisciplinary scientists with solid basic knowledge in molecular and material chemistry as well as engineering and technology. In catalysis education, the separation between catalysis science and catalysis technology is a regular issue, we believe that as proposed by Pagliaro new courses in catalysis science and technology should integrate a unified approach [38].

1.3 Origins of Supported Metal Single Atom Catalysts

Most recent reviews dealing with supported metal single atom catalysis underline the innovative character of this type of catalysis:

- *Single-atom catalysis is a recent discipline of heterogeneous catalysis* [16];
- *One of the earliest heterogeneous catalysts with surface metal atoms was reported in 1999* [12];
- *Single-atom catalysis is currently one of the most innovative and fastest growing research areas in the entire field of catalyst science* [14].

While it is true that most of the important work in the field dates from the twenty-first century [39], an analysis of the bibliography associating the words “single atoms” and “catalysis” in web of science (WoS) reveals that research had been initiated long before (Figure 1.4a). We will present below some of the pioneering works (sometimes forgotten) representative of this research (Figure 1.4b) and put them in perspective of certain recent (re)discoveries.

If the failure to obtain a high metal loading can be in certain cases a brake for the industrial development of SACs (for example in electrocatalysis) [40], for certain reactions at very high tonnages involving the use of noble metals, the catalyst must be lightly loaded for economic reasons. This is for example the case of reforming Pt/Al₂O₃ catalysts. A crucial invention was made in 1947 by Haensel at Universal Oil Products, who suggested the use of platinum supported on alumina as a bifunctional catalyst in the refining process [41]. Using such catalyst with an expensive metal for producing a cheap commodity sounded crazy to most of his contemporaries. However, Haensel and coworkers demonstrated that the high activity of a 0.01% Pt/Al₂O₃ catalyst combined with long-term stability and possible *in situ* regeneration justify a high initial price. In fact, this catalyst was economically more efficient in the long run than a “cheap” catalyst with a shorter life. Hydrogen adsorption indicated that 50% or more of the Pt atoms were surface atoms. This was the first industrial bifunctional catalyst, exposing both platinum SA and acid sites, and still today researches are conducted on supported Pt_{SA} as reforming catalysts [42–44]. A combination of nuclear magnetic resonance (NMR) spectroscopy, and high-angle annular dark-field scanning transmission

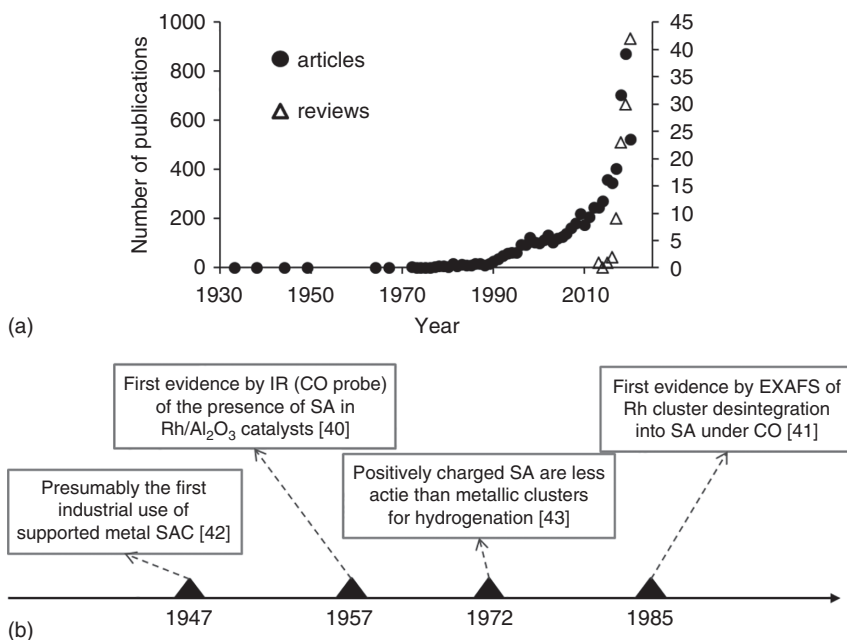


Figure 1.4 (a) Number of publications (research articles or review) per year obtained by the keywords “single atoms” and “catalysis” from Web of Science. Source: Web of Science. (b) Important findings related to supported metal single atom catalysis dating from the last century. Source: Philippe Serp.

electron microscopy (HAADF-STEM) analyses coupled with density functional theory (DFT) calculations was used to reveal the nature of anchoring sites of a catalytically active phase of Pt/ γ -Al₂O₃ catalyst [44]. At low (≤ 1 wt%) Pt loadings, Pt is atomically dispersed on the support surface, and coordinatively unsaturated Al³⁺ centers acts as binding sites for Pt_{SA}. Seventy years after Haensel et al. the group of Hutchings and researchers from Johnson Matthey followed a similar strategy to replace the conventional Hg/C acetylene hydrochlorination catalyst by an Au/C catalyst [45]. They set as a target an Au loading smaller than 0.25 wt%, since higher loadings were considered to be not economically viable. *In situ* X-ray absorption fine structure spectroscopy (EXAFS) experiments have definitively shown that the active catalyst predominantly comprises Au(I) isolated cationic species [46]. Pt_{SA}/C are also promising for this reaction [47]. These two examples show that the concept of SA catalysis is attractive, particularly in the context of sustainable technologies that will make use of critical metals, which are expensive and of limited availability.

Different studies were conducted in the 1970s–1980s on low loading M/Al₂O₃ catalysts (M = Co [48], Cr [49, 50], Re [51] and more particularly Rh) in order to try to elucidate: i) the nature of the metal species (SA [52], highly dispersed 2D phase [δ phase] [53] or clusters [54]/nanoparticles [NP]), ii) the reasons why chemisorption stoichiometries do not prevail for supported Rh catalysts [55], and iii) in some cases the reason of the difficult reduction of some metal species. We will discuss below the case of Rh/Al₂O₃. It was thought that Rh may be present on Al₂O₃ in the

form of 3D crystallites, 2D “rafts,” and/or isolated SA (ion) sites. This system was investigated by a variety of techniques including chemisorption [53, 55], infrared spectroscopy [56–62], X-ray photoelectron spectroscopy (XPS) [54], electron spin resonance (ESR) [54], EXAFS [52, 54, 63, 64], ^{13}C NMR spectroscopy [65, 66], luminescence spectroscopy [67], and ultra-high resolution electron microscopy [53]. Most of these techniques are still used today for the characterization of supported metal SA (*Chapter 5*). One of the most powerful techniques for the study of the surface chemistry of supported high surface area metal deposits is transmission infrared spectroscopy. The chemisorption of CO by Rh/Al₂O₃ has been well studied using infrared spectroscopy. Preliminary experiments performed by Garland and coworker [56] have shown that three main types of chemisorbed CO are produced on Rh/Al₂O₃ catalysts: (i) a single CO molecule adsorbed on one Rh atom, (ii) a band due to bridged CO, and (iii) two CO molecules adsorbed on one Rh atom (geminal dicarbonyl rhodium species). The latter surface species was particularly present for catalysts with a low Rh loading presenting highly dispersed rhodium species. The other two species are related to CO-covered Rh crystallites. The geminal dicarbonyl rhodium species was associated to a Rh(I) species, which cannot be completely reduced to Rh(0) even at 400 °C [60]. However, infrared (IR) analyses were not conclusive about the exact nature of this species and both monoatomically dispersed Rh(I) species on Al₂O₃ (Rh_{SA}/Al₂O₃), and 2D supported Rh “rafts” [53] were proposed. For the latter case, the geminal dicarbonyl rhodium species formed on the edge atoms of supported Rh “rafts.” Later on, an important finding was reported by Primet [68], who discovered that the geminal dicarbonyl species are not formed at low temperature, but develop on warming up to room temperature. Dissociation of CO was assumed on Rh(0), and CO in excess adsorbs on the surface Rh-O species to give the geminal dicarbonyl rhodium(I) species. EXAFS analyses were also conducted on reduced low loading catalysts [52, 54, 63, 64]. In such samples, the measured average coordination number was low (1.5 [52] to 4.9 [64] according to the temperature of reduction). Although the presence of isolated Rh⁺ ions in these low loading catalysts was not completely ruled out, it was proposed that they mainly contain small metal clusters, consisting of 6–10 atoms [54]. Another important finding was that adsorption of CO at room temperature changes the system completely. It results in a significant disruption of the Rh clusters, ultimately leading to the isolated Rh(I) geminal dicarbonyl species, in which Rh is surrounded by two CO and three oxygen ions. This study also confirmed that CO dissociation occurs and is followed by CO adsorption on the oxidized rhodium.

These results can be put into perspective with more recent results obtained in studies on supported metal SACs. First, several studies have been published on the role of CO on the stabilization of SA [69], but also on their (dynamic) formation by NP disintegration [70, 71] or reconstruction [72–74]. In particular, it was shown that for CO assisted Ostwald ripening and induced NP disintegration, the strong interaction between CO and the metal is essential [75]. When the formation of the metal–CO complexes becomes exothermic with respect to the supported metal NP of interest, the metal particles will be disintegrated to the individual SA.

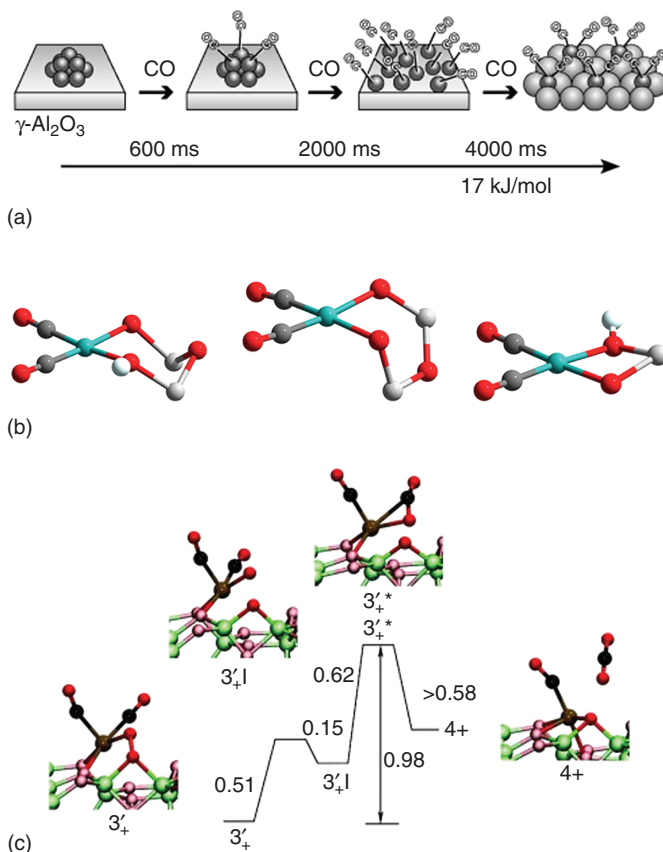


Figure 1.5 (a) An illustrative mechanism, with times given as taken from the beginning of the reaction, of three elementary steps at room temperature for the disintegration of Rh clusters on Al_2O_3 during CO adsorption by time-resolved DXAFS. Source: Suzuki et al. [70]. Reproduced with permission of Wiley-VCH; (b) Three types of connectivity of $\text{Rh}^{\text{I}}(\text{CO})_2$ species to the Al_2O_3 observed in the minimum energy geometries obtained by periodic DFT calculations. Source: Roscioni et al. [76]. Reproduced with permission of American Chemical Society; (c) Free energy profile obtained by DFT for CO oxidation on $\text{Rh}^{\text{I}}(\text{CO})_2/\text{Al}_2\text{O}_3$. Source: Ghosh et al. [77]. Reproduced with permission of Wiley-VCH.

Second, some studies on SAs are also dealing with the specific $\text{Rh}_{\text{SA}}/\text{Al}_2\text{O}_3$ system [70, 76, 77]. Thus, time-resolved energy-dispersive EXAFS analyses have revealed three steps for the structural rearrangement of Rh clusters (Figure 1.5a) [70]. Before CO exposure, Rh atoms in the cluster composed of seven Rh atoms in the first layer and three Rh atoms in the second layer interact with the surface oxygen atoms of the support. Each Rh atom in the lower layer interacts with two O atoms of the support. Then CO (0–600 ms) rapidly adsorbs on the cluster without Rh—Rh bond breaking. At the second step after 600 ms, further CO adsorption weakens the Rh—Rh bonds, and the Rh cluster is completely disintegrated at 3000 ms yielding the $[\text{Rh}(\text{CO})_2]$ monomer that interacts with three surface O atoms. The slowest step in the cluster

disintegration ($E_a = 4.1$ kcal/mol) is the formation of $[\text{Rh}(\text{CO})_2]$ monomers, which occurs concertedly with bond rearrangement at the interface, and probably with the oxidation of Rh^0 to Rh^+ by surface OH groups. It is important to place this result in the context of the characterization of supported metal SACs. Indeed, IR spectroscopy using CO as a probe molecule is regularly used to complement more local electron microscopy analyzes (Chapter 5) in order to distinguish SA, clusters or NP [78]. The fact that under CO some metallic clusters can disintegrate at room temperature at the second-scale can of course call into question many interpretations, and lead to errors or misunderstanding of the system. First principle plane-wave/DFT calculations were used to determine the exact environment of the $[\text{Rh}(\text{CO})_2]$ monomer. It was found that Rh_{SA} exhibit a square-planar coordination geometry [76], and is bound to two oxygen atoms of the support (Figure 1.5b) [76, 77]. Finally, the CO oxidation was investigated with this catalyst. CO oxidation over Rh_{NP} is a highly structure sensitive reaction. The observed structure sensitivity involves the formation and interplay of three structurally discrete supported Rh species; Rh_{NP} , a Rh_2O_3 -like phase, and monodisperse $\text{Rh}^{\text{I}}(\text{CO})_2$ species [79]. Thus, the reactivity of the $\text{Rh}^{\text{I}}(\text{CO})_2/\text{Al}_2\text{O}_3$ was investigated for the CO oxidation reaction by DFT (Figure 1.5c), and compared to that $\text{Rh}^0(\text{CO})_2/\text{Al}_2\text{O}_3$ and $\text{Rh}_6/\text{Al}_2\text{O}_3$ [77]. The computed activation energy for this reaction were 21.2 ($\text{Rh}^{\text{I}}(\text{CO})_2/\text{Al}_2\text{O}_3$), 9.7 ($\text{Rh}^0(\text{CO})_2/\text{Al}_2\text{O}_3$), and 27.4 kcal/mol ($\text{Rh}_6/\text{Al}_2\text{O}_3$). The CO oxidation on $\text{Rh}_6/\text{Al}_2\text{O}_3$ is sluggish compared to SA due to strong Rh—CO bonding on the cluster. For SA, the oxidation of Rh to Rh^{I} has a negative effect on the rate of CO oxidation, and the first CO oxidation by $\text{Rh}^0(\text{CO})_2$ is remarkably faster than that by $\text{Rh}^{\text{I}}(\text{CO})_2$, for which the free energy barriers are 9.7 and 21.2 kcal/mol, respectively.

It is worth mentioning the pioneering works of Köpp and coworkers, who investigated in the early 1970s the reactivity of Pd/C catalysts prepared by metal evaporation (Pd_{SA} or Pd_{NP}) for the reverse methane cracking reaction ($\text{C} + 2\text{H}_2 = \text{CH}_4$) [80, 81]. The results of their study on isosteric enthalpies of adsorption of hydrogen on atomically distributed Pd on carbon indicate that the occupation of H_2 molecules per Pd atom in SA catalysts was surprisingly small, and that the Pd_{SA} on the carbon are positively polarized ($\text{Pd}^{\delta+}$) [80]. Therefore, they could conclude that the high hydrogenation activity for the investigated reaction was due to Pd clusters and not due to Pd_{SA} . The fact that Pt_{SA} dispersed in sodalite cages cannot chemisorb hydrogen was also evidenced by Imelik and coworkers [82]. Three interpretations were proposed: (i) at least 2 Pt atoms are required to dissociate H_2 ; (ii) Pt_{SA} have lost their metallic properties including hydrogen chemisorption; and (iii) hydrogen chemisorption is inhibited because a partial electron transfer between Pt atoms and Lewis acid sites occurs. The poor efficiency of electron-deficient supported noble metal SACs for dihydrogen dissociation [83] (and further hydrogenation reactions) [84, 85] has been recently confirmed in different studies. In fact, several studies have shown that in the electron-deficient SA sites, the dissociation of H_2 followed a heterolytic pathway, whose barrier can be higher than that in metallic clusters with homolytic dissociation [86–90]. In that case, the electron depletion of metal SAs induces downshift of the d-band center of

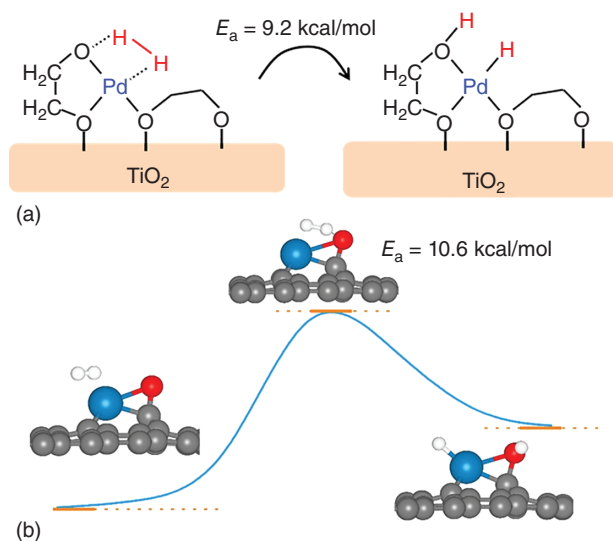


Figure 1.6 (a): Heterolytic dissociation of H_2 on EG-stabilized $\text{Pd}_{\text{SA}}/\text{TiO}_2$. Source: Philippe Serp. (b): Heterolytic dissociation of H_2 on $\text{Pd}_{\text{SA}}\text{-O/graphene}$. Source: Yan et al. [92]. Reproduced with permission of Elsevier.

the $\text{M}^{\delta+}$ species and consequently reduces, when compared with the metallic clusters/NP, the binding strength of the dissociatively adsorbed hydrogen atoms. This is particularly appealing for selective hydrogenation (see *Chapter 8*), since catalysts allowing activation of H_2 and weak adsorption strength of the dissociated H atoms can exhibit optimal efficiency in balancing activity and selectivity for the targeted product. On other side, if high hydrogenation activity is aimed, it is necessary to modify the local environment of the $\text{M}^{\delta+}$ species in order to facilitate the heterolytic dissociation of H_2 , or to favor a homolytic cleavage. Such strategies have been followed in some studies. A facilitated heterolytic dissociation of H_2 was obtained on $\text{Pd}_{\text{SA}}/\text{TiO}_2$ by doping the system with ethylene glycol (EG) [91], or by introducing oxygen functionalities on carbon in $\text{Pd}_{\text{SA}}/\text{C}$ catalysts (Figure 1.6b) [92, 93]. It is generally accepted that upon homolytic dissociation of H_2 on Pd_{NP} , hydrides ($\text{H}^{\delta-}$) are formed. When heterolytic activation of H_2 occurs, both $\text{H}^{\delta-}$ and $\text{H}^{\delta+}$ are produced that should allow better hydrogenation of polar unsaturated bonds. This was demonstrated in a study on EG-stabilized $\text{Pd}_{\text{SA}}/\text{TiO}_2$ catalysts. First, the presence of EG facilitates the heterolytic dissociation of H_2 (Figure 1.6a). Second, the authors observed a much superior catalytic performance by EG-stabilized $\text{Pd}_{\text{SA}}/\text{TiO}_2$ than conventional $\text{Pd}_{\text{NP}}/\text{C}$ catalysts in the hydrogenation of benzaldehyde. The activation of H_2 on $\text{Pd}_{\text{SA}}/\text{graphene}$ catalysts was investigated, for which the Pd_{SA} is located in a carbon vacancy [92–94]. If oxygen surface groups are not present in the vicinity of the Pd_{SA} , the hydrogen molecule becomes activated but the H—H bond is not broken. Thus, the electro-deficient Pd_{SA} is not able to dissociate the hydrogen molecule [94]. However, if an oxygen atom is present ($\text{Pd}_{\text{SA}}\text{-O/graphene}$), the reaction proceeds with an activation energy of 10.6 kcal/mol (Figure 1.6b).

To increase the electronic density on a $\text{Pt}^{\delta+}_{\text{SA}}$ immobilized on ceria, doping with phosphorus, an electron acceptor was proposed [95]. Such electronic interactions between the Pt_{SA} and the P-modulated neighboring oxygen atoms of the support led to a remarkable activity enhancement toward the hydrogenation of styrene, cyclohexene, phenylacetylene, and nitrobenzene. H. Lee and coworkers proposed a more straightforward solution that controls the oxidation state of Pt_{SA} in $\text{Pt}_{\text{SA}}/\text{CeO}_2\text{-Al}_2\text{O}_3$ catalysts by varying the reduction temperature [96]. Remarkably, the Pt_{SA} were stable up to 500 °C reduction temperature, clusters appearing at 600 °C. EXAFS and XPS analyses have shown that by increasing the reduction temperature from 100 to 500 °C, the oxidation state of Pt_{SA} could be controlled from highly oxidant (Pt^0 16.6%) to highly metallic (Pt^0 83.8%), while maintaining the SA structure.

The low activity of supported metal SAs compared to metal NPs for the reduction of nitric oxide by hydrogen was also experimentally evidenced in the 1970s and 1980s when studying the influence of metal loading in $\text{Rh}/\text{Al}_2\text{O}_3$ [97] and $\text{Pt}/\text{Al}_2\text{O}_3$ catalysts [98]. Two explanations were proposed. First, isolated SAs cannot offer an optimum site configuration for a transition complex, since the NO reduction requires at least two nitric oxide molecules and two hydrogen atoms, so that clusters with a minimum number of metal atoms are required for optimal activity. Second, the higher oxidation state of the metal in SAs due to strong interaction with the support is expected to result in a lower turnover frequency, as compared to a lower oxidation state of the metal in the particulate phase [98]. More recently, nitric oxide reduction with H_2 or CO was also investigated on supported metal SA [99–102]. First, in a study on reduction of NO with CO on Rh/SiO_2 catalysts, Tao and coworkers have confirmed that $\text{Rh}_{\text{SA}}/\text{SiO}_2$ are much less efficient than $\text{Rh}_{\text{NP}}/\text{SiO}_2$ for this reaction [99]. It was shown from DFT calculations that the significant difference in the reaction mechanisms between $\text{Rh}_{\text{SA}}/\text{SiO}_2$ and $\text{Rh}_{\text{NP}}/\text{SiO}_2$ is that NO can directly dissociatively chemisorb on Rh_{NP} due to the multiple adsorption sites; however, for $\text{Rh}_{\text{SA}}/\text{SiO}_2$, NO hardly dissociates with only one active site. This leads to much higher activity but also selectivity on Rh_{NP} in comparison to Rh_{SA} . Nickel SAs supported on g- C_3N_4 nanosheets shows a comparable reactivity with the $\text{Rh}_{\text{SA}}/\text{SiO}_2$ catalyst; i.e. complete NO conversion at around 450 °C [100]. An efficient strategy to overcome the limitations of supported single atoms for this reaction is to associate them with a second metal. This can be done either by using single metal alloys (*Chapter 4*) [101], or by diluting noble metal SAs in Co_3O_4 [102]. Thus, $\text{Cu}_5\text{Pd}_{\text{SA}}/\text{Al}_2\text{O}_3$ exhibited outstanding catalytic activity and N_2 selectivity in the reduction of NO by CO since complete conversion of NO to N_2 was achieved at 175 °C [101]. Kinetic and DFT studies demonstrated that the rate determining step (N—O bond breaking of the $(\text{NO})_2$ dimer) was promoted by the Pd_{SA} ($E_{\text{a}} = 11.4$ kcal/mol, to be compared to 25.6 kcal/mol computed for $\text{Ni}_{\text{SA}}/\text{g-}\text{C}_3\text{N}_4$) [100], while N_2O decomposition to N_2 smoothly proceeds on the Cu surface, which contributes to the excellent N_2 selectivity. The use of catalysts containing dispersed bimetallic sites Pt_1Co_m and Pd_1Co_n allowed performing the reduction of nitric oxide with hydrogen at temperature as low as 150 °C [102].

1.4 Challenges, Limitations, and Possible Opportunities in Supported Metal Single Atom Catalysis

The unique structural and electronic properties of supported metal SACs that result from multiple factors (unsaturated coordination environment, specific interaction between the SAs and its neighboring atoms) offer great potential in catalysis. All those merits are based on the stability of these catalysts that people are most concerned about. The potential of these catalysts has been explored in diverse thermo- (*Chapters 8–12*), electro- (*Chapter 13*), and photochemical (*Chapter 14*) applications ranging from small-molecule activation (*Chapter 10*) to the production of fine chemicals (*Chapter 12*). If the key factors controlling the activity, selectivity, and stability of this new class of catalysts are mastered (cf. discussion in the following sections of this chapter), thus 100% atom utilization efficiency can be expected. This is particularly appealing for the replacement of noble-metal-based catalysts for energy applications and of homogeneous catalysts in organic synthesis. However, despite 100% atom utilization efficiency, a general question regarding supported metal SA catalysts is whether a SA on a support represents the optimal structure to deliver the highest intrinsic catalytic activity for all reactions. The rate at which an elementary reaction proceeds on the catalyst surface will depend on the strength of reactants/products/intermediates – surface interaction (*electronic effects*), but also on the availability of specific atomic groupings (both in mono- and bimetallic/alloyed systems) that can provide the number of surface atoms necessary for chemisorption, by acting as active sites (*atomic ensemble effects*). In supported metal SA catalysts, if ligand (electronic) effects can be modulated, the so-called ensemble (geometric) effect, which is necessary for some reactions, is not present. Thus, they may be inactive for some complex catalytic reactions where multiple reactants, intermediates, and products are involved, unless the reaction proceeds via a distinct mechanism and/or the support itself can fulfill the required catalytic role. If such reactions are unwanted (undesired side reactions, coking), the isolation of the metallic atoms is a promising strategy [93, 103]. But if atomic ensemble effects are necessary for the aimed reaction to proceed (hydrogenolysis), single metal alloys or double, and triple metal atom catalysts should be preferred [104–106]. Alternatively, the creation of arrays of SAs has been proposed to overcome this limitation of supported metal SA catalysts while maintaining 100% atom utilization [107, 108].

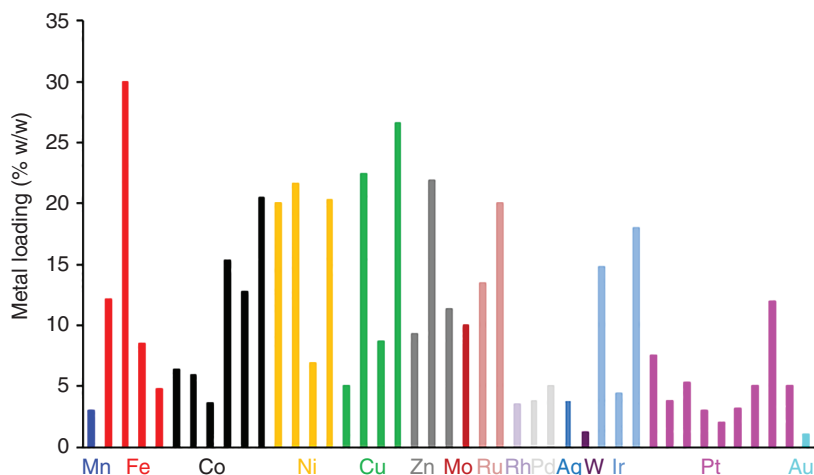
The grand challenge in the development of supported SACs is their low metal-atom loading density, uncontrollable localization and ambiguous interactions with supports, posing difficulty in maximizing their characterization and catalytic performances. The following sections will treat these different aspects of supported single-atom catalysis, highlighting the challenges, but also presenting the limitations and possible opportunities through representative examples.

1.4.1 Metal Loading in Supported Metal Single Atom Catalysts

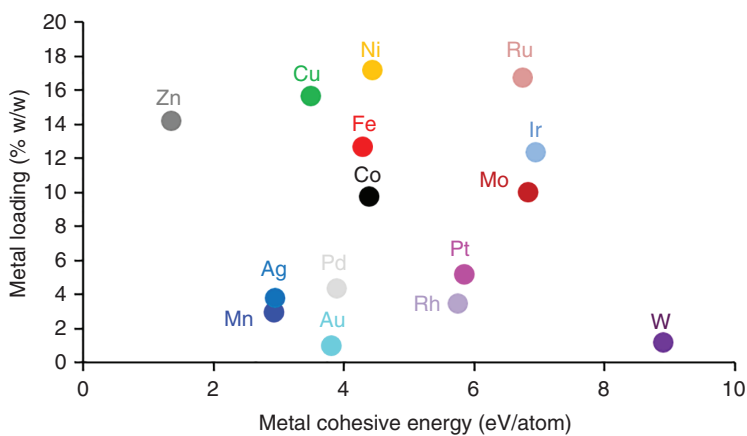
The low metal loadings generally needed to prevent metal NPs in supported metal SACs is generally presented as a brake on their industrial development. This is a

somewhat simplistic vision, which does not integrate the specificities of certain catalytic processes. Thus, we discuss in Section 1.3 the Platforming process developed by Haensel et al. [41], who understood that a Pt-based catalyst presenting a long life and could be regenerated and reused *in situ* would, in fact, be economically efficient. To achieve this goal with an expensive metal as Pt, it was mandatory to minimize the amount of platinum. In 1947, they showed that a catalyst with 0.01% platinum on alumina was both active and stable. Hutchings when looking for a gold catalyst to replace the mercury-based industrial catalyst for hydrochlorination of acetylene to produce vinyl chloride followed the same strategy [45]. Of course, if for some reactions the activities obtained with lightly loaded supported metal SACs are not sufficient, then the low loadings become a major handicap, because their use would imply increasing the size of the reactors, which is not economically sustainable. A current trend in catalysis being to replace noble metals (expensive and for some of them identified as critical elements) by 3d transition metals (Fe, Co, Ni for example), which are generally less active, it also becomes necessary to significantly increase the metal loading. Finally, some difficult reactions, i.e. the oxygen reduction reaction in proton exchange membrane fuel cells, require high loading of an expensive metal as Pt. If the current tendency in fuel cell electrocatalysis is to try to decrease as much as possible the Pt loading [109], significant efforts are still needed to reach the Pt amounts present in catalytic converters [110]. In this context, significant efforts have been made in recent years to increase the loading of single atoms in supported metal SACs (see *Chapters 2 and 3*). To prepare high loading supported metal SACs, three main aspects have to be considered: (i) large-scale synthesis is still challenging and new synthetic strategies should be explored; (ii) suitable metal precursors should be selected to ensure easy decomposition and stabilization; and (iii) the appropriate supports should present high density of potential anchoring sites and allow strong metal-support interactions. Pyrolysis and wet-chemistry methods are the most efficient ones up to now to reach high metal loadings (>5 wt% of metal) [40]. Pyrolysis techniques produce carbon-based catalysts with nitrogen-coordinated metal SA when zeolitic imidazolate frameworks nitrogen-enriched molecular carbon precursors are used as precursors [111–113]. The high temperatures used in these processes usually generate a random distribution of $M_{SA}-N-C$ sites on/in the carbon matrix (even if the $M-N_4$ environment characteristics of some metalloenzymes is often proposed) [114, 115] making the method relatively unpredictable and difficult to reproduce at the atomic level [113]. Furthermore, it is also worth noting that the exposure and accessibility of the metal SAs is also crucial to fulfill the 100% atomic utilization [116]. Incorporating metal into MOFs will undoubtedly buries some of the SAs deep inside the MOF framework, which would reduce atom utilization [117, 118].

Wet-chemistry routes (e.g. co-precipitation, impregnation) have been widely used to prepare supported metal SACs, due to their simple implementation and potential for large-scale production. To reach high metal loading by these methods, the choice of the support and the type of interaction with the SAs (coordination, electrostatic adsorption or ionic bonding) are crucial. Obviously, supports presenting a high density of well-defined anchoring sites should be preferred. In that context, the use of nitrogen-doped carbon materials such as graphitic carbon nitride is particularly



(a)



(b)

Figure 1.7 (a) Recent advances for supported metal SAC synthesis with high metal loadings. (b) Relation between the metal loading in high loading supported metal SAC and the cohesive energy of the bulk metal. Source: Philippe Serp.

interesting [119]. Other well-organized 2D materials such as hexagonal boron nitride (h-BN) or MoS₂ have also been used.

Figure 1.7a shows recent advances on supported metal SAC synthesis with high metal loadings for Mn [120], Fe [121–125], Co [122, 126–130], Ni [122, 127, 131–133], Cu [122, 134–136], Zn [122, 137, 138], Mo [139], Ru [85, 122], Rh [122, 140], Pd [122, 140, 141], Ag [142], W [143], Ir [122, 140, 144, 145], Pt [140, 146–152], and Au [153]. From this figure, it appears that relatively high metal loadings have been repeatedly obtained by different methods for some metals like Ni, whereas with some others like Pt or Pd, it seems difficult to reach such loadings. In order to explain this tendency, we try to correlate the average value of the (high) metal loading of Figure 1.7a with the cohesive energy of the metals. Indeed, we could expect that

metals with a high cohesive energy are difficult to stabilize in the form of isolated atoms, due to their natural tendency to form metal NPs. If high loading were indeed reported for Zn_{SA} catalysts, a metal that present a low cohesive energy; and low loading were reported for W_{SA} catalysts, a metal presenting a high cohesive energy, it is obvious from Figure 1.7b that no correlation really exists between these two parameters. For example, for a metal like ruthenium that presents a relatively high cohesive energy, high metal loadings were obtained by pyrolyzing coordinated polymers, producing Ru_{SA} (13.5 wt%) with a Ru–N environment [122]; or by a bottom up approach, producing Ru_{SA} (20% w/w) with a Ru–C environment [85]. Thus, in addition to the cohesive energy of the metal, the choice of the metal precursor/support couple, which will ultimately dictate the strength of the metal/support interaction must be carefully taken into consideration [154].

1.4.2 Metallic Species Homogeneity in Supported Metal Single Atom Catalysts

Two types of homogeneity can be considered when preparing a supported metal SAC. The first one deals with the selective deposition or not of metal SAs on the support (presence of clusters or NPs). The second one deals with the presence or not of a tailored local environment around the SA (SSHCs or not).

1.4.2.1 Are Clusters or Nanoparticles Present in Supported Metal Single Atom Catalysts?

As far as selective deposition of SAs (or double, triple atoms) is concerned, many synthetic strategies are at the disposal of the chemists (see *Chapters 2, 3, 4, and 15*). It is however important to ensure the homogeneity of the samples, in particular by checking the absence of clusters or nanoparticles. If microscopy offers a clear view, it nevertheless remains local, and analytical techniques offering an overview of the samples must be used in addition (*Chapter 5*). For this purpose, IR spectroscopy (with a probe molecule such as CO), EXAFS or XPS are commonly used. We would like to caution the reader here against the use of these techniques, as they can all present limitations to distinguish supported metal SA from clusters. We have already discussed in Section 1.3, the phenomenon of clusters disintegration under CO at room temperature, which can occur on the scale of the second. IR analyses at sub-ambient temperature is expected to be useful for identifying sample homogeneity, and monitoring possible catalyst reconstruction due to exposure of probe molecules via corollary *in-situ* or *ex-situ* scanning transmission electron microscopy (STEM) and X-ray absorption spectroscopy (XAS) characterization is critical for developing definitive probe molecule IR assignments [78]. For XPS analyses, first supported SACs present some challenges: they are often high surface area insulating powders and the metal loading can be very low (0.5 wt% or lower). In addition, new or inexperienced practitioners should avoid erroneous data collection and interpretation [155]. Finally, to make the distinction between SAs and clusters/NPs, the chemical state and most importantly the electronic state of the metal within a SA-containing material are probed by this technique. Thus, if a significant

charge transfer is present, the SA is often found to be electron-deficient ($M^{\delta+}$) [156], while the same metal in an NP will be at zero oxidation state (M^0). It is nevertheless important to note that significant charge transfer can also be measured in the case of clusters of low nuclearity [157–160], making the distinction between SAs and clusters very delicate. Synchrotron radiation-based EXAFS is typically used in combination with HAADF-STEM to identify the SAs. However, it was shown that, in many cases, EXAFS is not sensitive enough to identify SAs, which may easily confuse the contributions from clusters or small nanoparticles due to the polydispersity and disorder effects and similar spectral shape [161]. A very careful measurement by HAADF-STEM and detailed IR/XPS/EXAFS analyses with reasonable comparison to the control samples are thus highly required to thoroughly identify the SAs and distinguish them from clusters or small NPs. Finally, if selective production of supported metal SACs is often the goal to study their specific reactivity, it is important to note that mixtures of SAs and clusters/NPs are often present in commercial catalysts [162]. During a catalytic reaction, all these various “sites” may contribute differently to the observed catalytic performance. If the very large majority of catalytic studies on supported metal SACs are limited to a comparison of the reactivity of SAs with that of metallic NPs; some studies have already demonstrated possible synergy and cooperative catalysis between SAs and NP [163–169]. This is a subject that definitively deserves more study in the future, and in that context, the control of the SA/NP ratio in a given catalyst is also challenging.

1.4.2.2 Control of the Local Environment of Single Atoms in Supported Metal Single Atom Catalysts

Structural regulation of catalytic performances in supported metal SACs involved a control of metal-support interactions (charge state and coordination environment) [24, 170, 171]. These characteristics are playing together to induce steric and electronic effects to determine the catalytic performances of supported metal SACs, as for homogeneous metal catalysts. Of course, and like in homogeneous catalysis, the charge state of the metal can have a pronounced effect on the catalytic activity. The effect of overall charge (particularly of positive charge) on Rh and Ir metal compound reactivity was discussed by Crabtree [172]. He clearly showed that in some cases, overall charge is the major factor determining reactivity, independent of the nature of the ligands. The control of the charge state of a given metal in supported metal SACs can be achieved by changing the nature of the support, if of course the interaction established between the SA and the support has not a predominantly covalent polar nature [173]. Note also that in photo- or electrocatalysis, other characteristics of the support should also be taken in consideration, such as the value of the band gap and its electronic conductivity. Thus, it has been shown that Au_{SA} are positively charged ($Au(I)$) on TiO_2 and CeO_2 but negatively charged ($Au(0)$) on ZrO_2 , HfO_2 , and ThO_2 [174]. This support-dependent oxidation states and charge distribution of Au_{SA} can influence the reactivity toward CO. While CO adsorbs strongly on Au_{SA}/TiO_2 , a weaker adsorption occurs for Au_{SA}/ZrO_2 . But for a given support the control of the charge state of a given metal (and therefore its reactivity) can also be achieved by changing the nature of the exposed support

facet or adsorption site. For example, Au_{SA} on perfect CeO₂(111) are reported to be inactive for CO oxidation due to the formation of negatively charged Au at the oxygen vacancy [175], but Li and coworkers have shown that the CeO₂ support with step sites stabilizes Au_{SA} with a positively charge state of +I, which exhibits much higher reactivity than the Au_{NP} [73]. Similarly, on the (111) and (100) surfaces of CeO₂, a Pt_{SA} exists at an oxidation state of +IV (upon replacement of Ce⁴⁺), while on the (110) CeO₂ surface, it exhibits an oxidation state of +II due to the formation of surface peroxide O₂²⁻ species [176]. For CO oxidation, the order of reactivity follows Pt_{SA}/CeO₂(110) < Pt_{SA}/CeO₂(111)/(100); but for methanol oxidation the reactivity order is Pt_{SA}/CeO₂(100) > Pt_{SA}/CeO₂(110) > Pt_{SA}/CeO₂(111). Compared with Pt_{SA}/CeO₂(110) and Pt_{SA}/CeO₂(111), the Pt–O–Ce active interface over Pt_{SA}/CeO₂(110) exhibits the highest intensity of distortion, which was correlated to its high activity. This discussion highlights that the local binding environment plays also a defining role in the catalytic performance, and that for some reactions the charge state alone is insufficient to explain the catalytic activity. Indeed, many different geometries can coexist with similar charge state, and perhaps only one might be catalytically active.

As far as the control of the local environments around the SA is concerned, it is obvious that the ability to tailor the atomic-scale structure of the active site is going to be key going forward in the field of supported metal SACs [177]. Indeed, in the absence of a well-defined coordination sphere around the metal SA, prediction and tuning of catalytic activity with supported metal SAsC will be challenging if the charge state of the metal is not the most important parameter, which is of course system dependent.

Additionally, the applicability of the d-band center and charge states often used to analyze the catalytic activity of transition metal surfaces/clusters can be unsure for supported metal SAC. Indeed, the spatial structure and orientation of frontier orbitals that are closest to the Fermi level of supported metal SACs play also a key role. This has been nicely illustrated by DFT on a study on Au_{SA} deposited on various C₃N supports [178]. In Au_{SA}/C₃N, by modifying the C₃N support, Au_{SA} can exist with different coordination modes and charge states, including Au⁺, Au⁻, and Au⁽⁰⁾. Dioxygen and dihydrogen adsorption was investigated on these different species. Surprisingly, the Au_{SA}⁺ is more active for gas adsorption than Au_{SA}⁽⁰⁾ or Au_{SA}⁻. In fact, the value of adsorption energy increases with the reduction of the number of electrons on Au. This appears to contradict with common believes that Au_{SA}⁻ are more active to dissociate these molecules, since they can inject electronic density in the unoccupied antibonding molecular orbitals of the adsorbates (2π* for O₂ or σ* for H₂), which is essential for the dissociation of these molecules. The explanation of the difference of reactivity between the Au_{SA}⁻ and Au_{SA}⁺ species in this specific case is the nature of the frontier orbital. For Au_{SA}⁻ the d_{z²} orbital is the highest in energy (Figure 1.8a), and for Au_{SA}⁺ it is the d_{xy} (Figure 1.8b). The level of hybridization between the frontier orbitals of gold and the lowest unoccupied molecular orbital (LUMO) of the adsorbate dictates the binding energy in these two cases (see Figure 1.8 for the case of O₂). For Au_{SA}⁺, the frontier orbital is close to the Fermi level, Au_{SA}-O₂ hybridization is strong and the 2π* orbital of O₂ extends

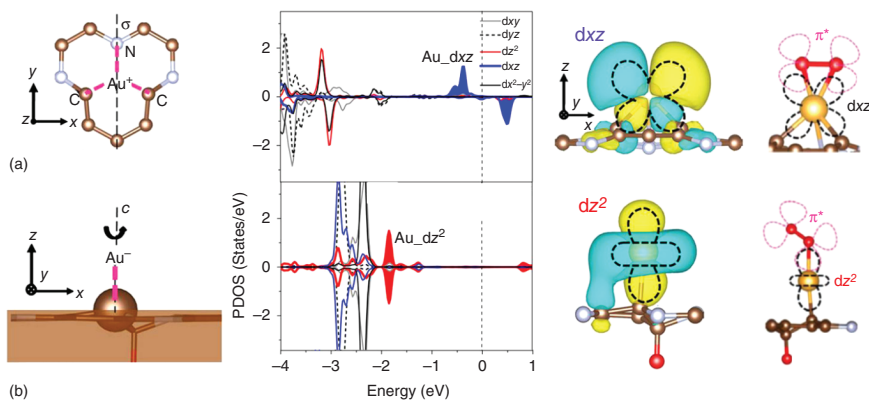


Figure 1.8 Projected density of states (PDOS) of Au d orbitals, calculated Wannier functions of frontier d orbitals of Au_{SA}, and different adsorption configurations of O₂ on Au_{SA} with two different frontier orbitals: (a) Au_{SA}⁺; and (b) Au_{SA}⁻ species. Source: Fu et al. [178]. Reproduced with permission of American Physical Society.

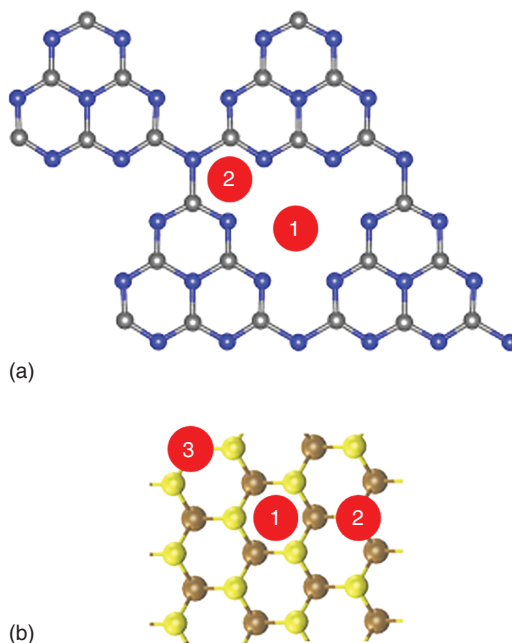
its tail to below the Fermi level and, hence, receives some electrons, even if Au is in a positively charged state. The partial occupation of the antibonding state certainly activates the dissociation of O₂, which is not the case for the Au_{SA}⁻ species. Thus, the ability of hybridizing with the 2π* orbital rather than the negative charge state of gold plays a major role in activating O₂ dissociation on these supported metal SACs.

Finally, beyond the control of the first coordination sphere, the control of the second sphere can also be important [24]. Indeed, atoms/functionalities in this second sphere can participate to the control of the activity [179] or the selectivity [180] of the supported metal SACs.

Various synthetic strategies have been developed for creating supported metal SACs with distinct coordination features. These include among others surface defect engineering, heteroatom doping, functional group grafting, spatial confinement, alloying, galvanic replacement or ionic liquid coating [170, 181, 182]. One exciting avenue is combining metal SA with some well-defined 2D materials such as g-C₃N₄ or MoS₂, with the aim to modulate the reactivity of metal atoms through unusual bonding- and electronic-environments. But even on these supports, different adsorption sites are present and both the nature of the adsorption site and energy of adsorption are metal dependent [183, 184]. Thus, the sixfold cavity of g-C₃N₄ is the energetically most favorable site for the deposition of SAs of Ti, Mn, Pd, Ag, Au, and W (site 1 on Figure 1.9a); while for Cr, Fe, Co, Ni, Cu, Mo, Ru, Rh, and Pt, the most favorable anchoring site is located at the corner of the sixfold cavity (site 2 on Figure 1.9a).

For MoS₂, it was found that, except for the Pd, Ag, and Au SAs, which adsorb preferentially on hollow (site 1 on Figure 1.9b), hollow, and topS sites (site 2 on Figure 1.9b), respectively, there is an energetic preference for the threefold top Mo adsorption sites (site 3 on Figure 1.9b). It is obvious that the research of “precise control” of the microenvironments of supported metal SACs is challenging, still at its infancy stage, but highly desired.

Figure 1.9 Adsorption sites for metal SAs on graphitic carbon nitride (a) and MoS₂ sheets (b). Source: Philippe Serp.



Another option consists in using bottom-up approaches. Thus, it is known that transition metal-metallofullerene can be produced easily by reacting the C₆₀ fullerene with metallic precursors providing C₆₀M_{SA} polymers with high metal loading [185–187]. These materials, which contain only metal SAs connected by C₆₀ with a well-defined coordination could constitute ideal candidates as model carbon-supported metal SACs.

Unfortunately, precise determination of the active site geometry on a real metal supported SAC is still extremely difficult; and it is thus probably fair to say that in general the primary source of local structural information in SACs is DFT-based calculations. Finally, we should mention that even if a precise location of metal SAs is achieved after the preparation of the catalyst, metal SA stability and dynamic should also be considered, as it will be discussed in Section 1.4.3.

1.4.3 Metal Single Atom Stability and Dynamic in Supported Metal Single Atom Catalysts

1.4.3.1 Thermal and Chemical Stability

The stability of supported metal SACs always comes into question because SAs, if bound only weakly to a support, are susceptible to aggregation either during catalyst pre-activation and/or reaction processes. Developing an active and stable supported metal SA catalyst is challenging due to the high surface free energy of metal atoms. For transition metals commonly used in catalysis, the energy difference (ΔE) between the cohesive energy between metal atoms in the bulk phase and the thermodynamic driving force to form SA-support bonds is generally positive, i.e. thermodynamically it is more favorable to form M—M bonds rather than M-support bonds.

For oxide supports, the ΔE values for Ru, Rh, Pd, Pt, and Au all lay within the range of 100–200 kJ/mol (Figure 1.10a) [188], implying that additional means of stabilization during or after the SA synthesis need to be considered for those metals. The intrinsic stability of SAs arises from the support-assisted lower chemical potential when compared to NPs. When the free-energy change from NPs to SAs is negative, NPs can be dispersed to SAs spontaneously, which leads to thermodynamic stability of SAs (Figure 1.10b, black line). Since the binding strength depends on the p-d coupling between the SA and the support, the stable metal supported SA requests strong p-d coupling and deep states, while the unbound states near Fermi level may weaken the stability. However, if the free-energy change is positive, the SAs will be stable only if the aggregation barrier is high enough to prevent sintering, which corresponds to the kinetic stability of SAs (Figure 1.10b, dotted line) [189].

Even though thermally stable supported metal SAs have been successfully produced using reducible supports prone to generate oxygen vacancies to stabilize SAs [149, 190–194], chemical stability issues due to the presence of oxidative or reducing reactants and high temperature under operating conditions should also be considered [195]. Generally, the more weakly the surface metal atom is attached to the support, the more strongly it binds small adsorbates [196]. Consequently, both thermodynamic and kinetic criteria have to be considered to determine the stability of supported metal SAs [189]. The thermodynamic part includes: (i) energetics of supported metal NPs, which is based on the Gibbs–Thomson relation with considering the adsorbed reactants; and (ii) the chemical potential of *monomers* (both the metal SA and SA-reactant complexes) on the support.

The kinetic part includes: (i) the diffusion barrier of monomers on perfect surfaces and defects; and (ii) the barrier of moving one metal atom from a supported metal NP to a substrate surface with corresponding sintering rate equations [73, 75].

CO stabilize a Pt_{SA} more than a Pt_{NP} because of the stronger adsorption of CO to a Pt_{SA} and also because only a fraction of the Pt atoms in an NP is covered by CO, as shown in Figure 1.10c. We already discussed in Section 1.2, the case of Rh_{NP} that spontaneously disintegrated into Rh_{SA} under CO at room temperature. But at higher temperature, the Rh complexes decomposed, and the Rh_{SA} released started to agglomerate and form metal NPs. Similarly, reactant-assisted ripening/disintegration had also been reported when supported metal NPs were exposed to dioxygen [197–201]. The reason was attributed to the formation of volatile oxygen–metal complexes [202]. Interestingly, Corma and coworkers have shown that by controlling the activation treatment (in that case under H_2 or O_2), it was possible to prepare catalysts in which the nature of the Pt species (Pt_{SA} formed under O_2 or Pt_{NP} formed under H_2) can be tuned reversibly [203]. Note that H_2 activation is not always associated to SA instability. Thus, the addition of H_2 is beneficial for the stabilization of $\text{Ir}_{\text{SA}}/\text{C}$ catalysts by suppressing the formation of volatile Ir complexes during methanol carbonylation to acetic acid [204]. Of course, metal supported SA formation by the disintegration of metallic NPs will be strongly dependent on NP density and the concentration of support defect sites [71, 205]. The energetics of supported NP/SA during Ostwald ripening and reactant assisted (here carbon monoxide-assisted) Ostwald ripening are presented in Figure 1.11a,b [75].

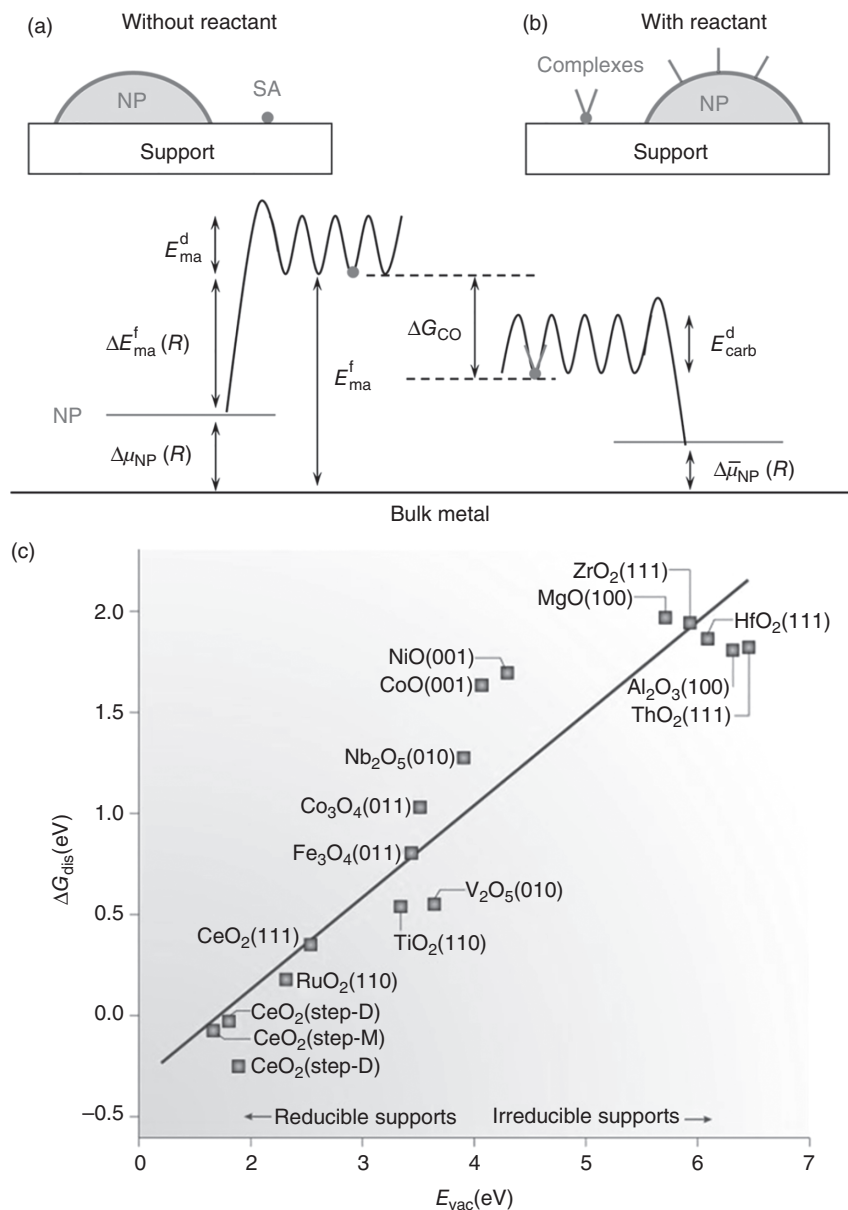


Figure 1.11 Energy diagram of supported NP/SA without (a) and with (b) the presence of CO. Here, $\Delta\mu_{NP}(R)$ and $\Delta\bar{\mu}_{NP}(R)$ are the chemical potentials of supported metal NP, E_{ma}^f and $\Delta E_{ma}^f(R)$ are the formation energies of monomers (the metal SA) on support with respect to infinite and finite size metal particle, ΔG_{CO} is the Gibbs free energy of adsorption of reactants CO on the metal SA, and E_{ma}^d and E_{carb}^d are the diffusion barriers of monomers (the metal SA and the SA-reactant complexes) on support. Source: Ouyang et al. [75]. Reproduced with permission of American Chemical Society. (c) The Gibbs free energy change for Au cluster disintegration (ΔG_{dis}) can be plotted against the energy associated with the formation of support vacancies (E_{vac}). The more reducible the support, the more stable the single Au centers are after dissociating from an Au cluster. Source: Wang et al. [12]. Reproduced with permission of Springer Nature.

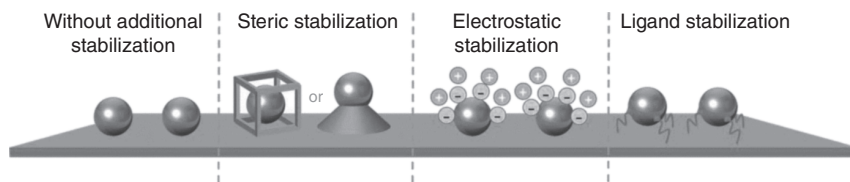


Figure 1.12 Schematic representation of stabilization principles in colloidal chemistry applicable to the synthesis of stable single-atom catalytic systems. Source: Hülsey et al. [188]. Reproduced with permission of Wiley VCH.

The first step of sintering by Ostwald ripening, i.e. the release of metal SAs from NPs is paradoxically the basis for metal redispersion in some specific cases. Ripening occurs when large thermodynamically stable NPs trap the metal SAs released by the smaller NPs after their fragmentation.

But if the support provides strong metal-support interactions such as those typically observed on reducible oxides (CeO_2 or TiO_2), the mobile metal SAs can be intercepted before further aggregation phenomena occur, limiting or even eliminating the problem (Figure 1.11c). In some cases, the support sites necessary for the enthalpic stabilization of SAs, for example O_v , can be formed *in situ* during the catalytic reaction, as shown in the case of Pd/ TiO_2 catalysts for the reverse water gas shift reaction [205].

If it appears obvious that the stability control in supported SACs should involve strong electronic metal-support interactions, other strategies have also been proposed, mainly based on knowledge originating from colloidal chemistry (Figure 1.12) [188]. Thus, electrostatic stabilization of supported SA catalysts by ionic liquids (ILs) provides sufficient protection to isolated SAs by increasing the kinetic barrier for the formation of metal–metal bonds on the support [206]. Employing a steric barrier during the reduction of the metal precursor, for example by iced photochemical reduction, led to the formation of SAs even in an aqueous solid matrix that can then be transferred and bind strongly to different supports [207].

Today, a growing body of evidence suggests that supported SAs through strong covalent bonds can be more stable than their NP counterparts and are even resistant to sintering during reactions at high temperatures. If several theoretical models have been developed to correlate the structural stability or catalytic activity with the adsorption strength of reaction intermediate, d-band center of transition metals, and e.g. filling number, and charge transfer ability, the simultaneous correlation of structural stability and catalytic activity with a specific parameter has not been reported so far. Simultaneous enhancement of thermostability and catalytic activity is thus questionable. An attempt was made by Liu and coworkers to obtain a rational description for structural stability and catalytic activity of supported SA catalysts (Figure 1.13) [208]. The parameters associated with competitive distribution of free electrons near the Fermi level should be considered during simultaneously combined optimization of structural stability and catalytic activity. The fully occupied bonding orbitals correspond to the stability between the SAs, and the authors addressed the relationship between the stability of supported SAs and the amount of free electrons near Fermi

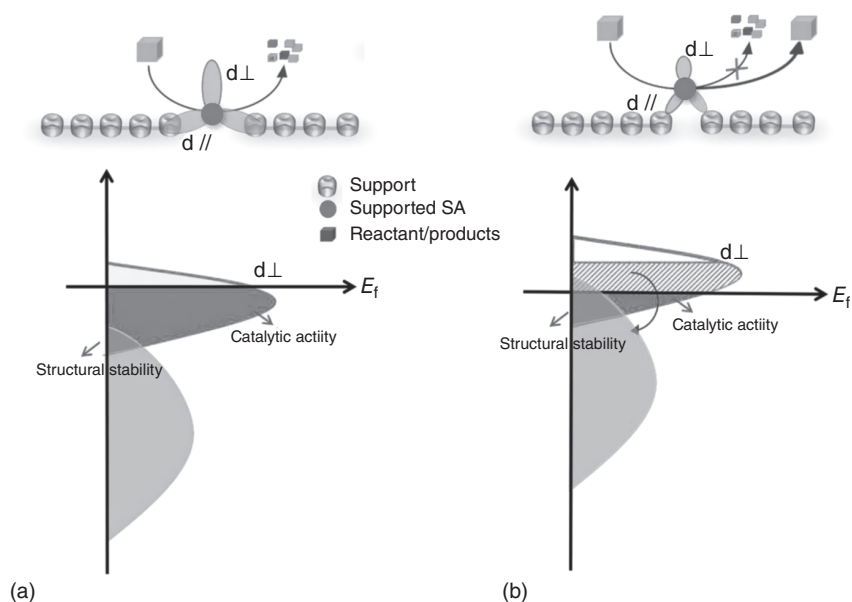


Figure 1.13 Illustration of competitive relationship between (a) catalytic activity and (b) structural stability of supported single atom catalysts. Source: Wang et al. [208]. Reproduced with permission of Elsevier.

level using the parameter of binding strength. The free electrons near Fermi level caused by unsaturated coordination can be responsible for the catalytic activity, and the relationship between catalytic activity and the densities of free electrons was considered to optimize the chemisorption. Compounds without such free electrons may not display excellent catalytic activity. Therefore, the SAs should be strongly coupled to the supports, and the localized structural coordination should be unsaturated to form a dangling bond near the Fermi level [209]. Thus, combining the conventional screening criteria of catalyst stability (formation energy) and catalytic activity (adsorption energy), for example by using high-throughput prediction and machine learning, can provide new insights into understanding and developing new supported SACs combining structural stability and high activity. Thus, combination of DFT calculations and various machine learning methods have already been used to investigate catalyst stability or reactivity [210–214]. Scaling relation between the diffusion activation barrier (E_a) of a metal SA on a support (a most relevant factor to its stability) and $(E_{\text{bind}})^2/E_c$ has been reported; where E_{bind} is the binding energy of the SA and E_c the metal cohesive energy [210].

1.4.3.2 Supported Single Atom Dynamics in Chemical Reactions

The structures of supported metal SACs may change during catalysis (dynamic evolution) because of well-known restructuring phenomena induced by chemical reactions and/or high temperatures. Understanding the dynamism of supported metal SACs under reaction conditions is important [215, 216], especially given the possible reversible dynamical conversion of NPs into SAs during catalysis.

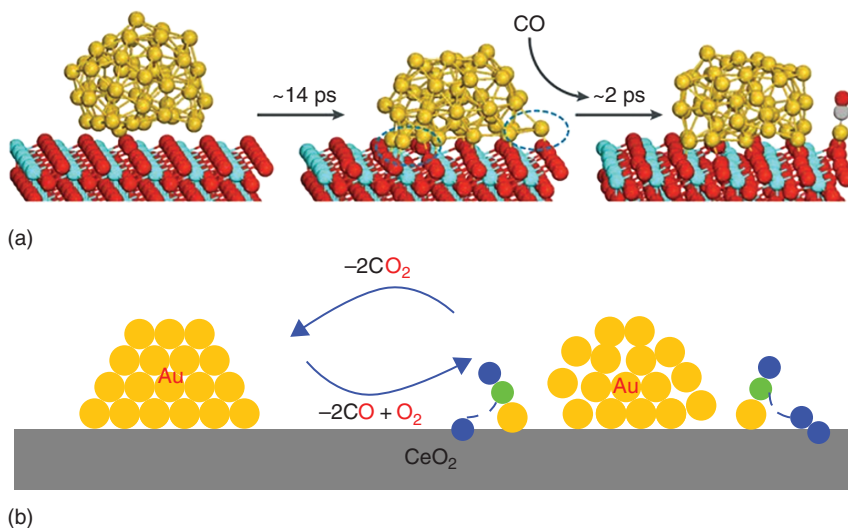


Figure 1.14 (a) Snapshots from a molecular dynamics simulation of a CeO₂-supported Au₅₀ cluster show that a Au_{SA} can dissociate from the cluster to bind CO. Source: Wang et al. [12]. Reproduced with permission of Springer Nature. (b) Schematic representation of the dynamic behavior at the interface during CO oxidation on Au/CeO₂ catalysts. Source: Wang et al. [72]. Springer Nature. CC BY 4.0.

Thus, dynamic (co)catalysis of Au_{SA} has been reported in the case of CO oxidation on Au/CeO₂ catalysts [72], and methane pyrolysis for producing carbon and dihydrogen on gold nanoparticles [217]. Rousseau and coworkers used *ab initio* molecular dynamics simulations to reveal dynamic SA catalytic mechanism for the CO oxidation by CeO₂-supported gold clusters [72]. The dynamic SA catalytic mechanism results from the ability of Au^{δ+} species to strongly couple with the redox properties of CeO₂ in a synergistic manner, thereby lowering the energy of redox reactions. The Au^{δ+} can break away from the Au_{NP} (Figure 1.14a) to catalyze CO oxidation, adjacent to the metal/oxide interface and subsequently reintegrate back into the NP after the reaction is completed (Figure 1.14b).

Such a dynamic phenomenon is reminiscent of that observed in the case of Pd_{NP} for carbon–carbon coupling reactions [218, 219]. Interestingly, on Pt_{SA}/Al₂O₃ catalysts, a reverse phenomenon was observed [220]. It was first shown that the Pt_{SA}/Al₂O₃ catalysts are poorly active for CO oxidation. However, the Pt_{SA} gradually and irreversibly convert into highly active Pt clusters throughout the heating-cooling reaction cycles, even under highly oxidizing conditions favorable to atomic dispersion. Similarly, the *in situ* transformation of isolated Cu_{SA}N₄ into Cu clusters (the real active species) has been evidenced during the electrocatalytic reduction of CO₂ into ethanol [221]. Interestingly, the Cu clusters redispersed into isolated Cu_{SA} following exposure to air. These two latter studies show that care must be taken before concluding on the nature of the active sites in supported metal SACs, even at very low metal loading. Experimental evidence for the co-catalysis

between Au_{SA} and Au_{NP} was also evidenced during methane pyrolysis [217]. It was demonstrated that Au_{NP} surface partially disintegrate, releasing Au_{SA} . DFT calculations have shown that the Au_{SA} could co-catalyze the reaction with Au_{NP} . Moreover, the Au_{SA} dynamically aggregate into Au_{NP} , which re-disintegrate back to Au_{SA} .

Another important dynamic phenomenon in supported metal SACs is the change of local coordination environments and/or oxidation states/charge transfer that can occur during the reaction process. A limited number of studies deal with this important point. Dynamic charge and oxidation state of $\text{Pt}_{\text{SA}}/\text{CeO}_2$ catalysts were examined by combining DFT and first-principles molecular dynamics by N. López and coworkers [222]. The authors also demonstrated how the reactivity for CO oxidation is closely related to this dynamic behavior. Their work raises the question of the common assignment of a fixed oxidation state in supported metal SACs, which is an oversimplification. Indeed, several well-defined charge states that were dynamically interconnected depending on the Pt– CeO_2 combination and thus coexist were identified. $\text{Pt}^{2+}\text{-4O}$ was the resting state of the material under most conditions; and only after CO (or H_2) treatment a significant pressure, the Pt–4O coordination was reduced to Pt–3O. The Pt–3O system is labile and converts into Pt–2O in <0.5 ps at room temperature. During the CO oxidation cycle on Pt–2O, the electronic structure of the active site needs to be dynamic to allow both CO adsorption (occurring at ionic Pt) and oxidation (occurring on Pt^0) elementary steps in the mechanism. Three Pt oxidation states coexist on Pt–2O (Pt^0 47% total lifetime, Pt^{1+} 49% total lifetime and Pt^{2+} 4% total lifetime). When CO is adsorbed, the new intermediate shows larger lifetimes for the ionic Pt configurations (Pt^{1+} 36% total lifetime and Pt^{2+} 63% total lifetime). Then, O_2 can adsorb, forming a species for which the formal oxidation state of the metal is Pt^{2+} , regardless of its previous state. From this configuration on, CO_2 formation easily pushes the system to the low-lying Pt^0 state (Figure 1.15).

This dynamic evolution of the metal oxidation states reminds the concept of non-innocent ligands in coordination [223–225] or bioinorganic [226] chemistry. This type of ligands is either redox-active (“redox non-innocent”) or actively involved in bond-making or -breaking processes (“chemically non-innocent”), and contribute to ligand-mediated oxidation state changes. Structural evolution of atomically dispersed $\text{Pt}_{\text{SA}}/\text{TiO}_2$ catalysts was also evidenced through a combination of *in situ* atomic-resolution microscopy and spectroscopy based characterizations, and supported by first-principles calculations [227]. It was demonstrated that Pt_{SA} can adopt a range of local coordination environments and oxidation states, which evolve in response to varied environmental conditions, similarly to the dynamic behavior of copper species ions in zeolites [228]. This variation in local coordination and electronic state of Pt species showed a strong influence on the catalytic performance for CO oxidation on systems where the Pt_{SA} active site was adsorbed at well-defined locations on the support. It was proposed, based on EXAFS and STEM analyses and DFT calculations that oxidation of $\text{Pt}_{\text{SA}}/\text{TiO}_2$ resulted in Pt substituting into the Ti_{6c} position ($\text{Pt}^{4+}_{\text{Ti6c}}$); mild reduction pulled Pt_{SA} out of the lattice to form $\text{Pt}^{+2}\text{-O}_2$ species; and harsh reduction induced the formation of $\text{Pt}^{+1}\text{-OH}$ species that were mobile and adsorbed to both step and terrace sites on the support (Figure 1.16). It was expected that these changes were driven not only by Pt_{SA} energetics, but also by structural transformations of reducible TiO_2

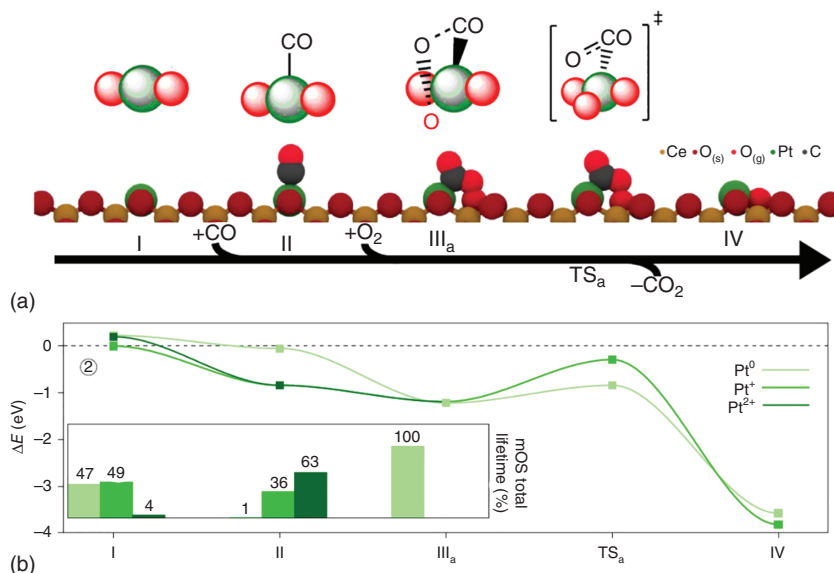


Figure 1.15 (a) Side views of the reaction steps of CO oxidation. Dark red denotes oxygen from the bulk phase (s) and bright red denotes oxygen from the gas phase (g). (b) Reaction profile of CO oxidation for each oxidation state of Pt. Source: Daelman et al. [222]. Reproduced with permission of Springer Nature.

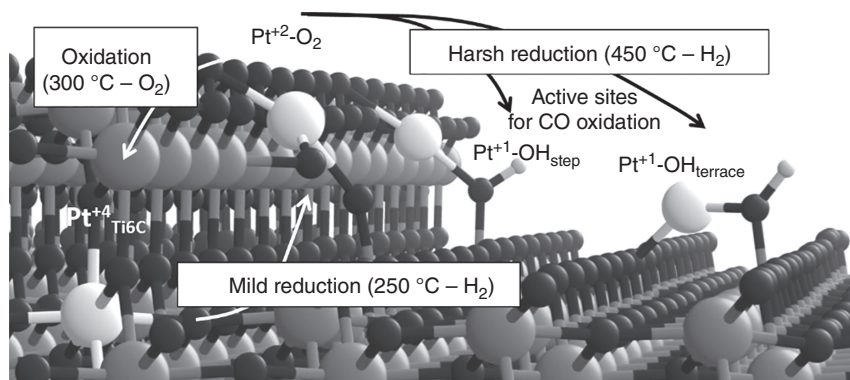


Figure 1.16 Schematic showing the proposed dynamic evolution of Pt_{SA}/TiO₂ catalysts following oxidation, mild reduction, and harsh reduction. Structures were derived from DFT calculations and are consistent with experimental data. Source: DeRita et al. [227]. Reproduced with permission of Springer Nature.

support. Following harsh reduction, Pt_{SA} sites showed an increase in activity for CO oxidation of two to fivefold, depending on temperature, compared to Pt_{SA} sites that have followed oxidation or mild reduction [227].

Direct observation by synchronous illumination XPS of dynamic bond evolution in Pt_{SA}/C₃N₄ catalysts during photocatalytic water splitting was also reported by Bi and coworkers [229].

The graphitic C_3N_4 support containing electron-rich N atoms provides sufficient sites to stabilize Pt^{2+}_{SA} through the formation of Pt—N bonds. The authors investigated the charge transfer and chemical bond evolution of such catalyst under light irradiation. The dynamic variations of Pt—N bond cleavage into Pt^0 and C=N bond could be experimentally observed under light irradiation. This transformation implies that in excitation states, the Pt^0 and C_3N_4 should be in separated states without any bonding, and only spatial confinement effects and van der Waals forces may insure the anchoring of the Pt_{SA} atoms on the support under light irradiation. Therefore, in excitation states, the electron-rich Pt_{SA}^0 atoms and the hole-rich C_3N_4 layers in separated states could participate in water reduction and oxidation, respectively.

These few examples clearly show that an improved understanding and description of dynamic behaviors, especially under operating conditions, will be invaluable.

1.4.4 Obtaining Reliable Information About the Active Sites of Metal SACs

Homogeneous catalysts present the advantage of well-defined single-active site on a molecular level. Supramolecular catalysts have been dominated by enzyme-inspired approaches; i.e. the assembly of catalytic species by harnessing multiple weak intramolecular interactions. In enzymatic catalysis, the simple model often used to describe enzyme activity is known as the lock-and-key model in which enzymes accelerate reactions by providing a tight-fitting area, known as the active site, where substrate molecules can react. For these latter systems, identification of the active site is more complex and relies more and more on computational approaches [230, 231]. In the case of supported metal SACs, obviously some similarities exist with homogeneous or enzymatic catalysis, but also some differences, which make that obtaining reliable information about the active site is complex. The first difficulty arise from the fact that most (if not all) of the supported metal SACs are not SSHCs. Furthermore, there is a possibility that the coordinated atom(s) of the support would be involved in the reactions as a co-catalytic site. Another important aspect to take into consideration is the intrinsic nature of the ligands, a molecular species in one case and a solid for supported metal SACs. Indeed, this solid can present redox properties, be constituted by a second metal, be a platform for reactant diffusion or for spillover (see Figure 1.1); all this richness, this diversity but also complexity are not present, or to a lesser extent in homogeneous catalysis with molecular complexes. In that context, the use of model supports, presenting few and well-defined anchoring possibilities for the metal should be encouraged [156].

We already discussed in this chapter the potentials and limitations of spectroscopic techniques for supported metal SACs, and they are further developed in *Chapter 5*. The advantages of *in situ/operando* techniques for capturing the reaction intermediates, identifying the active sites, and even monitoring the dynamic behaviors of both the geometric structure and electronic environment of catalytic sites in supported metal SACs should of course be considered [216, 232, 233]. They are discussed in *Chapter 6*. Finally, the coupling of spectroscopic studies with modeling

works is today a prerequisite to the understanding of the nature of the active site. Combinations of DFT and molecular dynamics and related computational algorithms have already been used with success (see *Chapter 7*) [234]. However, the interaction between the environment and the reaction intermediate species, which plays an important role in the exploration of catalytic mechanisms, is often neglected. Therefore, multiscale computational modeling approach should be developed.

Acknowledgments

This work was supported by the Agence Nationale de la Recherche (project ANR-19-CE07-0030), which is gratefully acknowledged.

References

- 1 Lykhach, Y., Kozlov, S.M., Skála, T. et al. (2016). Counting electrons on supported nanoparticles. *Nature Materials* 15 (3): 284–288. <https://doi.org/10.1038/nmat4500>.
- 2 Binninger, T., Schmidt, T.J., and Kramer, D. (2017). Capacitive electronic metal-support interactions: outer surface charging of supported catalyst particles. *Physical Review B* 96 (16): 165405. <https://doi.org/10.1103/PhysRevB.96.165405>.
- 3 Jia, X., Zhang, X., Rui, N. et al. (2019). Structural effect of Ni/ZrO₂ catalyst on CO₂ methanation with enhanced activity. *Applied Catalysis B: Environmental* 244: 159–169. <https://doi.org/10.1016/j.apcatb.2018.11.024>.
- 4 Lv, C., Xu, L., Chen, M. et al. (2020). Recent progresses in constructing the highly efficient Ni based catalysts with advanced low-temperature activity toward CO₂ methanation. *Frontiers in Chemistry* 8 (269) <https://doi.org/10.3389/fchem.2020.00269>.
- 5 Marzke, R.F. (1979). Quantum size effects in small metallic particles. *Catalysis Reviews* 19 (1): 43–65. <https://doi.org/10.1080/03602457908065100>.
- 6 Strizhak, P.E. (2013). Nanosize effects in heterogeneous catalysis. *Theoretical and Experimental Chemistry* 49 (1): 2–21. <https://doi.org/10.1007/s11237-013-9297-7>.
- 7 Che, M. and Bennett, C.O. (1989). The influence of particle size on the catalytic properties of supported metals. In: *Advances in Catalysis*, vol. 36 (eds. D.D. Eley, H. Pines and P.B. Weisz), 55–172. Academic Press.
- 8 Van Santen, R.A. (2009). Complementary structure sensitive and insensitive catalytic relationships. *Accounts of Chemical Research* 42 (1): 57–66. <https://doi.org/10.1021/ar800022m>.
- 9 Vogt, C., Groeneveld, E., Kamsma, G. et al. (2018). Unravelling structure sensitivity in CO₂ hydrogenation over nickel. *Nature Catalysis* 1 (2): 127–134. <https://doi.org/10.1038/s41929-017-0016-y>.

- 10 Sarma, B.B., Plessow, P.N., Agostini, G. et al. (2020). Metal-specific reactivity in single-atom catalysts: CO oxidation on 4d and 5d transition metals atomically dispersed on MgO. *Journal of the American Chemical Society* 142 (35): 14890–14902. <https://doi.org/10.1021/jacs.0c03627>.
- 11 Yang, X.-F., Wang, A., Qiao, B. et al. (2013). Single-atom catalysts: a new frontier in heterogeneous catalysis. *Accounts of Chemical Research* 46 (8): 1740–1748. <https://doi.org/10.1021/ar300361m>.
- 12 Wang, A., Li, J., and Zhang, T. (2018). Heterogeneous single-atom catalysis. *Nature Reviews Chemistry* 2 (6): 65–81. <https://doi.org/10.1038/s41570-018-0010-1>.
- 13 Liu, L. and Corma, A. (2018). Metal catalysts for heterogeneous catalysis: from single atoms to nanoclusters and nanoparticles. *Chemical Reviews* 118 (10): 4981–5079. <https://doi.org/10.1021/acs.chemrev.7b00776>.
- 14 Mitchell, S., Thomas, J.M., and Pérez-Ramírez, J. (2017). Single atom catalysis. *Catalysis Science & Technology* 7 (19): 4248–4249. <https://doi.org/10.1039/C7CY90090B>.
- 15 Kaiser, S.K., Chen, Z., Faust, A.D. et al. (2020). Single-atom catalysts across the periodic table. *Chemical Reviews* <https://doi.org/10.1021/acs.chemrev.0c00576>.
- 16 Samantaray, M.K., D’Elia, V., Pump, E. et al. (2020). The comparison between single atom catalysis and surface organometallic catalysis. *Chemical Reviews* 120 (2): 734–813. <https://doi.org/10.1021/acs.chemrev.9b00238>.
- 17 Cui, X., Li, W., Ryabchuk, P. et al. (2018). Bridging homogeneous and heterogeneous catalysis by heterogeneous single-metal-site catalysts. *Nature Catalysis* 1 (6): 385–397. <https://doi.org/10.1038/s41929-018-0090-9>.
- 18 Chen, F., Jiang, X., Zhang, L. et al. (2018). Single-atom catalysis: bridging the homo- and heterogeneous catalysis. *Chinese Journal of Catalysis* 39 (5): 893–898. [https://doi.org/10.1016/S1872-2067\(18\)63047-5](https://doi.org/10.1016/S1872-2067(18)63047-5).
- 19 Liu, F., Yang, T., Yang, J. et al. (2019). Bridging the homogeneous-heterogeneous divide: modeling spin for reactivity in single atom catalysis. *Frontiers in Chemistry* 7 (219) <https://doi.org/10.3389/fchem.2019.00219>.
- 20 Liu, P. and Zheng, N. (2018). Coordination chemistry of atomically dispersed catalysts. *National Science Review* 5 (5): 636–638. <https://doi.org/10.1093/nsr/nwy051>.
- 21 Jørgensen, C.K. (1966). Differences between the four halide ligands, and discussion remarks on trigonal-bipyramidal complexes, on oxidation states, and on diagonal elements of one-electron energy. *Coordination Chemistry Reviews* 1 (1): 164–178. [https://doi.org/10.1016/S0010-8545\(00\)80170-8](https://doi.org/10.1016/S0010-8545(00)80170-8).
- 22 van der Vlugt, J.I. (2019). Radical-type reactivity and catalysis by single-electron transfer to or from redox-active ligands. *Chemistry – A European Journal* 25 (11): 2651–2662. <https://doi.org/10.1002/chem.201802606>.
- 23 Wodrich, M.D. and Hu, X. (2017). Natural inspirations for metal–ligand cooperative catalysis. *Nature Reviews Chemistry* 2 (1): 0099. <https://doi.org/10.1038/s41570-017-0099>.

- 24 Qin, R., Liu, K., Wu, Q. et al. (2020). Surface coordination chemistry of atomically dispersed metal catalysts. *Chemical Reviews* **120** (21): 11810–11899. <https://doi.org/10.1021/acs.chemrev.0c00094>.
- 25 Hülsey, M.J., Lim, C.W., and Yan, N. (2020). Promoting heterogeneous catalysis beyond catalyst design. *Chemical Science* **11** (6): 1456–1468. <https://doi.org/10.1039/C9SC05947D>.
- 26 Passos, A.R., Rochet, A., Manente, L.M. et al. (2020). Three-dimensional strain dynamics govern the hysteresis in heterogeneous catalysis. *Nature Communications* **11** (1): 4733. <https://doi.org/10.1038/s41467-020-18622-2>.
- 27 Khorshidi, A., Violet, J., Hashemi, J. et al. (2018). How strain can break the scaling relations of catalysis. *Nature Catalysis* **1** (4): 263–268. <https://doi.org/10.1038/s41929-018-0054-0>.
- 28 Zhao, K., Zhu, Y., Shi, J. et al. (2019). Synergetic effects of strain engineering and substrate defects on generating highly efficient single-atom catalysts for CO oxidation. *Journal of Materials Chemistry A* **7** (15): 9297–9304. <https://doi.org/10.1039/C9TA01326A>.
- 29 Kohen, A. (2015). Role of dynamics in enzyme catalysis: substantial versus semantic controversies. *Accounts of Chemical Research* **48** (2): 466–473. <https://doi.org/10.1021/ar500322s>.
- 30 Narayanan, C., Bernard, D.N., Bafna, K. et al. (2018). Ligand-induced variations in structural and dynamical properties within an enzyme superfamily. *Frontiers in Molecular Biosciences* **5** (54) <https://doi.org/10.3389/fmolb.2018.00054>.
- 31 Kahraman, A. and Thornton, J.M. (2008). Methods to characterize the structure of enzyme binding sites. *Computational Structural Biology*: 189–221.
- 32 Brown, C.J., Toste, F.D., Bergman, R.G. et al. (2015). Supramolecular catalysis in metal–ligand cluster hosts. *Chemical Reviews* **115** (9): 3012–3035. <https://doi.org/10.1021/cr4001226>.
- 33 Serp, P. (2021). Cooperativity in supported metal single atom catalysis. *Nanoscale* **13**: 5985–6004. <https://doi.org/10.1039/D1NR00465D>.
- 34 Thomas, J.M., Raja, R., and Lewis, D.W. (2005). Single-site heterogeneous catalysts. *Angewandte Chemie International Edition* **44** (40): 6456–6482. <https://doi.org/10.1002/anie.200462473>.
- 35 Liu, J. (2017). Catalysis by supported single metal atoms. *ACS Catalysis* **7** (1): 34–59. <https://doi.org/10.1021/acscatal.6b01534>.
- 36 Thomas, J.M. (2019). The periodic table, zeolites and single-site heterogeneous catalysts. In: *The Periodic Table II: Catalytic, Materials, Biological and Medical Applications* (ed. D.M.P. Mingos), 37–52. Cham: Springer International Publishing.
- 37 Rogge, S.M.J., Bavykina, A., Hajek, J. et al. (2017). Metal–organic and covalent organic frameworks as single-site catalysts. *Chemical Society Reviews* **46** (11): 3134–3184. <https://doi.org/10.1039/C7CS00033B>.
- 38 Pagliaro, M. (2020). *laquo*Catalysis: a unified approach: a new course in catalysis science and technology. *Journal of Flow Chemistry* **11**: 53–58. <https://doi.org/10.1007/s41981-020-00100-x>.

- 39 Mitchell, S. and Pérez-Ramírez, J. (2020). Single atom catalysis: a decade of stunning progress and the promise for a bright future. *Nature Communications* 11 (1): 4302. <https://doi.org/10.1038/s41467-020-18182-5>.
- 40 Wu, J., Xiong, L., Zhao, B. et al. (2020). Densely populated single atom catalysts. *Small Methods* 4 (2): 1900540. <https://doi.org/10.1002/smt.201900540>.
- 41 National Academy of Engineering (2016). *Memorial Tributes*, vol. 20, 394. Washington, DC: The National Academies Press.
- 42 Liu, Y., Li, Z., Yu, Q. et al. (2019). A general strategy for fabricating isolated single metal atomic site catalysts in Y zeolite. *Journal of the American Chemical Society* 141 (23): 9305–9311. <https://doi.org/10.1021/jacs.9b02936>.
- 43 Zhang, S., Chen, L., Qi, Z. et al. (2020). Insights into the mechanism of n-hexane reforming over a single-site platinum catalyst. *Journal of the American Chemical Society* 142 (39): 16533–16537. <https://doi.org/10.1021/jacs.0c07911>.
- 44 Kwak, J.H., Hu, J., Mei, D. et al. (2009). Coordinatively unsaturated Al³⁺ centers as binding sites for active catalyst phases of platinum on γ -Al₂O₃. *Science* 325 (5948): 1670–1673. <https://doi.org/10.1126/science.1176745>.
- 45 Johnston, P., Carthey, N., and Hutchings, G.J. (2015). Discovery, development, and commercialization of gold catalysts for acetylene hydrochlorination. *Journal of the American Chemical Society* 137 (46): 14548–14557. <https://doi.org/10.1021/jacs.5b07752>.
- 46 Malta, G., Kondrat, S.A., Freakley, S.J. et al. (2017). Identification of single-site gold catalysis in acetylene hydrochlorination. *Science* 355 (6332): 1399–1403. <https://doi.org/10.1126/science.aal3439>.
- 47 Kaiser, S.K., Fako, E., Manzocchi, G. et al. (2020). Nanostructuring unlocks high performance of platinum single-atom catalysts for stable vinyl chloride production. *Nature Catalysis* 3 (4): 376–385. <https://doi.org/10.1038/s41929-020-0431-3>.
- 48 Yao, H.C. and Bettman, M. (1976). On the existence of two phases of cobalt oxide on a zirconia support. *Journal of Catalysis* 41 (3): 349–358. [https://doi.org/10.1016/0021-9517\(76\)90235-9](https://doi.org/10.1016/0021-9517(76)90235-9).
- 49 Poole, C.P. and MacIver, D.S. (1967). The physical-chemical properties of chromia-alumina catalysts. In: *Advances in Catalysis*, vol. 17 (eds. D.D. Eley, H. Pines and P.B. Weisz), 223–314. Academic Press.
- 50 O'Reilly, D.E. and MacIver, D.S. (1962). Electron paramagnetic resonance absorption of chromia—alumina catalysts¹. *The Journal of Physical Chemistry* 66 (2): 276–281. <https://doi.org/10.1021/j100808a021>.
- 51 Yao, H.C. and Shelef, M. (1976). Surface interactions in the system $\text{Re}\gamma\text{-Al}_2\text{O}_3$. *Journal of Catalysis* 44 (3): 392–403. [https://doi.org/10.1016/0021-9517\(76\)90416-4](https://doi.org/10.1016/0021-9517(76)90416-4).
- 52 Via, G.H., Meitzner, G., Lytle, F.W. et al. (1983). Extended X-ray absorption fine structure (EXAFS) of highly dispersed rhodium catalysts. *The Journal of Chemical Physics* 79 (3): 1527–1529. <https://doi.org/10.1063/1.445945>.
- 53 Yates, D.J.C., Murrell, L.L., and Prestridge, E.B. (1979). Ultradispersed rhodium rafts: their existence and topology. *Journal of Catalysis* 57 (1): 41–63. [https://doi.org/10.1016/0021-9517\(79\)90042-3](https://doi.org/10.1016/0021-9517(79)90042-3).

- 54 Van't Blik, H.F.J., Van Zon, J.B.A.D., Huizinga, T. et al. (1985). Structure of rhodium in an ultradispersed rhodium/alumina catalyst as studied by EXAFS and other techniques. *Journal of the American Chemical Society* 107 (11): 3139–3147. <https://doi.org/10.1021/ja00297a020>.
- 55 Yao, H.C., Japar, S., and Shelef, M. (1977). Surface interactions in the system RhAl_2O_3 . *Journal of Catalysis* 50 (3): 407–418. [https://doi.org/10.1016/0021-9517\(77\)90053-7](https://doi.org/10.1016/0021-9517(77)90053-7).
- 56 Yang, C. and Garland, C.W. (1957). Infrared studies of carbon monoxide chemisorbed on rhodium. *The Journal of Physical Chemistry* 61 (11): 1504–1512. <https://doi.org/10.1021/j150557a013>.
- 57 Yao, H.C. and Rothschild, W.G. (1978). Infrared spectra of chemisorbed CO on $\text{Rh}/\gamma\text{-Al}_2\text{O}_3$: site distributions and molecular mobility. *The Journal of Chemical Physics* 68 (11): 4774–4780. <https://doi.org/10.1063/1.435657>.
- 58 Yates, J.T. Jr., Duncan, T.M., and Vaughan, R.W. (1979). Infrared spectroscopic study of activated surface processes: CO chemisorption on supported Rh. *The Journal of Chemical Physics* 71 (10): 3908–3915. <https://doi.org/10.1063/1.438159>.
- 59 Yates, J.T. Jr., Duncan, T.M., Worley, S.D. et al. (1979). Infrared spectra of chemisorbed CO on Rh. *The Journal of Chemical Physics* 70 (3): 1219–1224. <https://doi.org/10.1063/1.437603>.
- 60 Rice, C.A., Worley, S.D., Curtis, C.W. et al. (1981). The oxidation state of dispersed Rh on Al_2O_3 . *The Journal of Chemical Physics* 74 (11): 6487–6497. <https://doi.org/10.1063/1.440987>.
- 61 Cavanagh, R.R. and Jr, J.T.Y. (1981). Site distribution studies of Rh supported on Al_2O_3 —An infrared study of chemisorbed CO. *The Journal of Chemical Physics* 74 (7): 4150–4155. <https://doi.org/10.1063/1.441544>.
- 62 Yates, J.T. Jr., and Kolasinski, K. (1983). Infrared spectroscopic investigation of the rhodium gem-dicarbonyl surface species. *The Journal of Chemical Physics* 79 (2): 1026–1030. <https://doi.org/10.1063/1.445844>.
- 63 Van't Blik, H.F.J., Van Zon, J.B.A.D., Huizinga, T. et al. (1983). An extended X-ray absorption fine structure spectroscopy study of a highly dispersed rhodium/aluminum oxide catalyst: the influence of carbon monoxide chemisorption on the topology of rhodium. *The Journal of Physical Chemistry* 87 (13): 2264–2267. <https://doi.org/10.1021/j100236a002>.
- 64 Van Zon, J., Koningsberger, D.C., van't Blik, H.F.J., and Sayers, D.E. (1985). An EXAFS study of the structure of the metal–support interface in highly dispersed $\text{Rh}/\text{Al}_2\text{O}_3$ catalysts. *The Journal of Chemical Physics* 82 (12): 5742–5754. <https://doi.org/10.1063/1.448563>.
- 65 Duncan, T.M. and Root, T.W. (1988). Adsorbed states of carbon monoxide on dispersed metals: quantitative analysis with carbon-13 NMR spectroscopy. *The Journal of Physical Chemistry* 92 (15): 4426–4432. <https://doi.org/10.1021/j100326a036>.
- 66 Robbins, J.L. (1986). Rhodium dicarbonyl sites on alumina surfaces. 1. Preparation and characterization of a model system. *The Journal of Physical Chemistry* 90 (15): 3381–3386. <https://doi.org/10.1021/j100406a016>.

- 67 Cooper, W.F. and Parker, W.L. (1989). Luminescent detection of Rh⁺ in supported metal catalysts. *Chemical Physics Letters* 156 (5): 463–466. [https://doi.org/10.1016/S0009-2614\(89\)87312-9](https://doi.org/10.1016/S0009-2614(89)87312-9).
- 68 Primet, M. (1978). Infrared study of CO chemisorption on zeolite and alumina supported rhodium. *Journal of the Chemical Society, Faraday Transactions 1: Physical Chemistry in Condensed Phases* 74: 2570–2580. <https://doi.org/10.1039/F19787402570>.
- 69 Kauppinen, M.M., Melander, M.M., and Honkala, K. (2020). First-principles insight into CO hindered agglomeration of Rh and Pt single atoms on m-ZrO₂. *Catalysis Science & Technology* 10 (17): 5847–5855. <https://doi.org/10.1039/D0CY00413H>.
- 70 Suzuki, A., Inada, Y., Yamaguchi, A. et al. (2003). Time scale and elementary steps of CO-induced disintegration of surface rhodium clusters. *Angewandte Chemie International Edition* 42 (39): 4795–4799. <https://doi.org/10.1002/anie.200352318>.
- 71 Goodman, E.D., Johnston-Peck, A.C., Dietze, E.M. et al. (2019). Catalyst deactivation via decomposition into single atoms and the role of metal loading. *Nature Catalysis* 2 (9): 748–755. <https://doi.org/10.1038/s41929-019-0328-1>.
- 72 Wang, Y.-G., Mei, D., Glezakou, V.-A. et al. (2015). Dynamic formation of single-atom catalytic active sites on ceria-supported gold nanoparticles. *Nature Communications* 6 (1): 6511. <https://doi.org/10.1038/ncomms7511>.
- 73 Liu, J.-C., Wang, Y.-G., and Li, J. (2017). Toward rational design of oxide-supported single-atom catalysts: atomic dispersion of gold on ceria. *Journal of the American Chemical Society* 139 (17): 6190–6199. <https://doi.org/10.1021/jacs.7b01602>.
- 74 Su, Y.-Q., Wang, Y., Liu, J.-X. et al. (2019). Theoretical approach to predict the stability of supported single-atom catalysts. *ACS Catalysis* 9 (4): 3289–3297. <https://doi.org/10.1021/acscatal.9b00252>.
- 75 Ouyang, R., Liu, J.-X., and Li, W.-X. (2013). Atomistic theory of ostwald ripening and disintegration of supported metal particles under reaction conditions. *Journal of the American Chemical Society* 135 (5): 1760–1771. <https://doi.org/10.1021/ja3087054>.
- 76 Roscioni, O.M., Dyke, J.M., and Evans, J. (2013). Structural characterization of supported RhI(CO)₂/γ-Al₂O₃ catalysts by periodic DFT calculations. *The Journal of Physical Chemistry C* 117 (38): 19464–19470. <https://doi.org/10.1021/jp405549k>.
- 77 Ghosh, T.K. and Nair, N.N. (2013). Rh1/γ-Al₂O₃ single-atom catalysis of O₂ activation and CO oxidation: mechanism, effects of hydration, oxidation state, and cluster size. *ChemCatChem* 5 (7): 1811–1821. <https://doi.org/10.1002/cctc.201200799>.
- 78 Asokan, C., DeRita, L., and Christopher, P. (2017). Using probe molecule FTIR spectroscopy to identify and characterize Pt-group metal based single atom catalysts. *Chinese Journal of Catalysis* 38 (9): 1473–1480. [https://doi.org/10.1016/S1872-2067\(17\)62882-1](https://doi.org/10.1016/S1872-2067(17)62882-1).

- 79 Newton, M.A., Dent, A.J., Diaz-Moreno, S. et al. (2006). Rapid monitoring of the nature and interconversion of supported catalyst phases and of their influence upon performance: CO oxidation to CO₂ by γ -Al₂O₃ supported Rh catalysts. *Chemistry A European Journal* 12 (7): 1975–1985. <https://doi.org/10.1002/chem.200500644>.
- 80 Gentsch, H., Guillen, N., and Köpp, M. (1972). Isostere Adsorptionsenthalpien von Wasserstoff an atomar verteiltem Palladium und Platin auf Kohle. *Zeitschrift für Physikalische Chemie* 82 (1-4): 49. <https://doi.org/10.1524/zpch.1972.82.1-4.049>.
- 81 Gentsch, H., Härtel, V., and Köpp, M. (1971). Heterogene Katalyse mit Ni- und Pd-Atomen. Methanbildung aus Kohlenstoff und Wasserstoff. *Berichte der Bunsengesellschaft für Physikalische Chemie* 75 (10): 1086–1092. <https://doi.org/10.1002/bbpc.19710751024>.
- 82 Gallezot, P., Alarcon-Diaz, A., Dalmon, J.A. et al. (1975). Location and dispersion of platinum in PtY zeolites. *Journal of Catalysis* 39 (3): 334–349. [https://doi.org/10.1016/0021-9517\(75\)90299-7](https://doi.org/10.1016/0021-9517(75)90299-7).
- 83 Cabria, I., López, M.J., Fraile, S. et al. (2012). Adsorption and dissociation of molecular hydrogen on palladium clusters supported on graphene. *The Journal of Physical Chemistry C* 116 (40): 21179–21189. <https://doi.org/10.1021/jp305635w>.
- 84 Rossell, M.D., Caparrós, F.J., Angurell, I. et al. (2016). Magnetite-supported palladium single-atoms do not catalyse the hydrogenation of alkenes but small clusters do. *Catalysis Science & Technology* 6 (12): 4081–4085. <https://doi.org/10.1039/C6CY00596A>.
- 85 Rivera-Cárcamo, C., Leng, F., Gerber, I.C. et al. (2020). Catalysis to discriminate single atoms from subnanometric ruthenium particles in ultra-high loading catalysts. *Catalysis Science & Technology* 10 (14): 4673–4683. <https://doi.org/10.1039/D0CY00540A>.
- 86 Doudin, N., Yuk, S.F., Marcinkowski, M.D. et al. (2019). Understanding heterolytic H₂ cleavage and water-assisted hydrogen spillover on Fe₃O₄(001)-supported single palladium atoms. *ACS Catalysis* 9 (9): 7876–7887. <https://doi.org/10.1021/acscatal.9b01425>.
- 87 Righi, G., Magri, R., and Selloni, A. (2019). H₂ dissociation on noble metal single atom catalysts adsorbed on and doped into CeO₂ (111). *The Journal of Physical Chemistry C* 123 (15): 9875–9883. <https://doi.org/10.1021/acs.jpcc.9b00609>.
- 88 Bi, Q., Yuan, X., Lu, Y. et al. (2020). One-step high-temperature-synthesized single-atom platinum catalyst for efficient selective hydrogenation. *Research*: 9140841. <https://doi.org/10.34133/2020/9140841>.
- 89 Ye, T.-N., Xiao, Z., Li, J. et al. (2020). Stable single platinum atoms trapped in sub-nanometer cavities in 12CaO·7Al₂O₃ for chemoselective hydrogenation of nitroarenes. *Nature Communications* 11: 1020. <https://doi.org/10.1038/s41467-019-14216-9>.

- 90 Lou, Y., Wu, H., and Liu, J. (2019). Nanocarbon-edge-anchored high-density Pt atoms for 3-nitrostyrene hydrogenation: strong metal-carbon interaction. *iScience* 13: 190–198. <https://doi.org/10.1016/j.isci.2019.02.016>.
- 91 Liu, P., Zhao, Y., Qin, R. et al. (2016). Photochemical route for synthesizing atomically dispersed palladium catalysts. *Science* 352 (6287): 797–800. <https://doi.org/10.1126/science.aaf5251>.
- 92 Yan, H., Lv, H., Yi, H. et al. (2018). Understanding the underlying mechanism of improved selectivity in pd_1 single-atom catalyzed hydrogenation reaction. *Journal of Catalysis* 366: 70–79. <https://doi.org/10.1016/j.jcat.2018.07.033>.
- 93 Yan, H., Cheng, H., Yi, H. et al. (2015). Single-atom Pd1/graphene catalyst achieved by atomic layer deposition: remarkable performance in selective hydrogenation of 1,3-butadiene. *Journal of the American Chemical Society* 137 (33): 10484–10487. <https://doi.org/10.1021/jacs.5b06485>.
- 94 Granja-DelRío, A., Alonso, J.A., and López, M.J. (2017). Competition between palladium clusters and hydrogen to saturate graphene vacancies. *The Journal of Physical Chemistry C* 121 (20): 10843–10850. <https://doi.org/10.1021/acs.jpcc.6b12018>.
- 95 Ma, Y., Chi, B., Liu, W. et al. (2019). Tailoring of the proximity of platinum single atoms on CeO_2 using phosphorus boosts the hydrogenation activity. *ACS Catalysis* 9 (9): 8404–8412. <https://doi.org/10.1021/acscatal.9b01536>.
- 96 Jeong, H., Shin, D., Kim, B.-S. et al. (2020). Controlling the oxidation state of Pt single atoms for maximizing catalytic activity. *Angewandte Chemie International Edition* 59 (46): 20691–20696. <https://doi.org/10.1002/anie.202009776>.
- 97 Yao, H.C., Yao, Y.F.Y., and Otto, K. (1979). Effects of the surface structure of $\text{Rh}\gamma\text{-Al}_2\text{O}_3$ on the hydrogenolysis of n-pentane, on the oxidation of n-butane, and on the reduction of nitric oxide. *Journal of Catalysis* 56 (1): 21–31. [https://doi.org/10.1016/0021-9517\(79\)90084-8](https://doi.org/10.1016/0021-9517(79)90084-8).
- 98 Otto, K. and Yao, H.C. (1980). The reduction of nitric oxide by hydrogen over $\text{Pt}\gamma\text{-Al}_2\text{O}_3$ as a function of metal loading. *Journal of Catalysis* 66 (1): 229–236. [https://doi.org/10.1016/0021-9517\(80\)90025-1](https://doi.org/10.1016/0021-9517(80)90025-1).
- 99 Zhang, S., Tang, Y., Nguyen, L. et al. (2018). Catalysis on singly dispersed Rh atoms anchored on an inert support. *ACS Catalysis* 8 (1): 110–121. <https://doi.org/10.1021/acscatal.7b01788>.
- 100 Zhang, L., Zhang, J., Qi, M. et al. (2020). First-principles investigation of single-atom Ni-g- C_3N_4 as an efficient catalyst for direct reduction of NO with CO. *Energy & Fuels* 34 (10): 12792–12799. <https://doi.org/10.1021/acs.energyfuels.0c01908>.
- 101 Xing, F., Jeon, J., Toyao, T. et al. (2019). A Cu–Pd single-atom alloy catalyst for highly efficient NO reduction. *Chemical Science* 10 (36): 8292–8298. <https://doi.org/10.1039/C9SC03172C>.
- 102 Nguyen, L., Zhang, S., Wang, L. et al. (2016). Reduction of nitric oxide with hydrogen on catalysts of singly dispersed bimetallic sites Pt_1Co_m and Pd_1Co_n . *ACS Catalysis* 6 (2): 840–850. <https://doi.org/10.1021/acscatal.5b00842>.
- 103 Nakaya, Y., Hirayama, J., Yamazoe, S. et al. (2020). Single-atom Pt in intermetallics as an ultrastable and selective catalyst for propane

- dehydrogenation. *Nature Communications* 11 (1): 2838. <https://doi.org/10.1038/s41467-020-16693-9>.
- 104** Pan, Y., Zhang, C., Liu, Z. et al. (2020). Structural regulation with atomic-level precision: from single-atomic site to diatomic and atomic interface catalysis. *Matter* 2 (1): 78–110. <https://doi.org/10.1016/j.matt.2019.11.014>.
- 105** Zhao, Y., Yang, K.R., Wang, Z. et al. (2018). Stable iridium dinuclear heterogeneous catalysts supported on metal-oxide substrate for solar water oxidation. *Proceedings of the National Academy of Sciences of the United States of America* 115 (12): 2902–2907. <https://doi.org/10.1073/pnas.1722137115>.
- 106** Li, X., Zhong, W., Cui, P. et al. (2016). Design of efficient catalysts with double transition metal atoms on C₂N layer. *The Journal of Physical Chemistry Letters* 7 (9): 1750–1755. <https://doi.org/10.1021/acs.jpcclett.6b00096>.
- 107** Wang, H., Liu, J.-X., Allard, L.F. et al. (2019). Surpassing the single-atom catalytic activity limit through paired Pt-O-Pt ensemble built from isolated Pt1 atoms. *Nature Communications* 10 (1): 3808. <https://doi.org/10.1038/s41467-019-11856-9>.
- 108** Qi, K., Cui, X., Gu, L. et al. (2019). Single-atom cobalt array bound to distorted 1T MoS₂ with ensemble effect for hydrogen evolution catalysis. *Nature Communications* 10 (1): 5231. <https://doi.org/10.1038/s41467-019-12997-7>.
- 109** Ganesan, A. and Narayanasamy, M. (2019). Ultra-low loading of platinum in proton exchange membrane-based fuel cells: a brief review. *Materials for Renewable and Sustainable Energy* 8 (4): 18. <https://doi.org/10.1007/s40243-019-0156-x>.
- 110** Kongkanand, A., Gu, W., and Mathias, M.F. (2019). Proton-exchange membrane fuel cells with low-Pt content. In: *Fuel Cells and Hydrogen Production: A Volume in the Encyclopedia of Sustainability Science and Technology*, 2e (eds. T.E. Lipman and A.Z. Weber), 323–342. New York: Springer New York.
- 111** Jiao, L. and Jiang, H.-L. (2019). Metal–organic-framework-based single-atom catalysts for energy applications. *Chem* 5 (4): 786–804. <https://doi.org/10.1016/j.chempr.2018.12.011>.
- 112** Han, A., Wang, B., Kumar, A. et al. (2019). Recent advances for MOF-derived carbon-supported single-atom catalysts. *Small Methods* 3 (9): 1800471. <https://doi.org/10.1002/smt.201800471>.
- 113** Hou, C.-C., Wang, H.-F., Li, C. et al. (2020). From metal–organic frameworks to single/dual-atom and cluster metal catalysts for energy applications. *Energy & Environmental Science* 13 (6): 1658–1693. <https://doi.org/10.1039/C9EE04040D>.
- 114** Jiao, L., Yan, H., Wu, Y. et al. (2020). When nanozymes meet single-atom catalysis. *Angewandte Chemie International Edition* 59 (7): 2565–2576. <https://doi.org/10.1002/anie.201905645>.
- 115** Wu, W., Huang, L., Wang, E. et al. (2020). Atomic engineering of single-atom nanozymes for enzyme-like catalysis. *Chemical Science* 11 (36): 9741–9756. <https://doi.org/10.1039/D0SC03522J>.
- 116** Li, M., Wang, H., Luo, W. et al. (2020). Heterogeneous single-atom catalysts for electrochemical CO₂ reduction reaction. *Advanced Materials* 32 (34): 2001848. <https://doi.org/10.1002/adma.202001848>.

- 117 Ye, Y., Cai, F., Li, H. et al. (2017). Surface functionalization of ZIF-8 with ammonium ferric citrate toward high exposure of Fe-N active sites for efficient oxygen and carbon dioxide electroreduction. *Nano Energy* 38: 281–289. <https://doi.org/10.1016/j.nanoen.2017.05.042>.
- 118 Wan, X., Liu, X., Li, Y. et al. (2019). Fe–N–C electrocatalyst with dense active sites and efficient mass transport for high-performance proton exchange membrane fuel cells. *Nature Catalysis* 2 (3): 259–268. <https://doi.org/10.1038/s41929-019-0237-3>.
- 119 Fu, J., Wang, S., Wang, Z. et al. (2020). Graphitic carbon nitride based single-atom photocatalysts. *Frontiers of Physics* 15 (3): 33201. <https://doi.org/10.1007/s11467-019-0950-z>.
- 120 Li, J., Chen, M., Cullen, D.A. et al. (2018). Atomically dispersed manganese catalysts for oxygen reduction in proton-exchange membrane fuel cells. *Nature Catalysis* 1 (12): 935–945. <https://doi.org/10.1038/s41929-018-0164-8>.
- 121 Zhao, L., Zhang, Y., Huang, L.-B. et al. (2019). Cascade anchoring strategy for general mass production of high-loading single-atomic metal-nitrogen catalysts. *Nature Communications* 10 (1): 1278. <https://doi.org/10.1038/s41467-019-09290-y>.
- 122 Xiong, Y., Sun, W., Xin, P. et al. (2020). Gram-scale synthesis of high-loading single-atomic-site Fe catalysts for effective epoxidation of styrene. *Advanced Materials* 32 (34): 2000896. <https://doi.org/10.1002/adma.202000896>.
- 123 Lu, C., Chen, Y., Yang, Y. et al. (2020). Single-atom catalytic materials for lean-electrolyte ultrastable lithium–sulfur batteries. *Nano Letters* 20 (7): 5522–5530. <https://doi.org/10.1021/acs.nanolett.0c02167>.
- 124 Lei, J., Liu, H., Yin, D. et al. (2020). Boosting the loading of metal single atoms via a bioconcentration strategy. *Small* 16 (10): 1905920. <https://doi.org/10.1002/smll.201905920>.
- 125 Yi, J.-D., Xu, R., Wu, Q. et al. (2018). Atomically dispersed iron–nitrogen active sites within porphyrinic triazine-based frameworks for oxygen reduction reaction in both alkaline and acidic media. *ACS Energy Letters* 3 (4): 883–889. <https://doi.org/10.1021/acsenergylett.8b00245>.
- 126 Yin, P., Yao, T., Wu, Y. et al. (2016). Single cobalt atoms with precise N-coordination as superior oxygen reduction reaction catalysts. *Angewandte Chemie International Edition* 55 (36): 10800–10805. <https://doi.org/10.1002/anie.201604802>.
- 127 Cheng, Y., Zhao, S., Johannessen, B. et al. (2018). Atomically dispersed transition metals on carbon nanotubes with ultrahigh loading for selective electrochemical carbon dioxide reduction. *Advanced Materials* 30 (13): 1706287. <https://doi.org/10.1002/adma.201706287>.
- 128 Li, Y., Wu, J., Zhang, B. et al. (2020). Fast conversion and controlled deposition of lithium (poly)sulfides in lithium-sulfur batteries using high-loading cobalt single atoms. *Energy Storage Materials* 30: 250–259. <https://doi.org/10.1016/j.ensm.2020.05.022>.
- 129 Li, J., Liu, H., Wang, M. et al. (2019). Boosting oxygen reduction activity with low-temperature derived high-loading atomic cobalt on nitrogen-doped

- graphene for efficient Zn-air batteries. *Chemical Communications* 55 (3): 334–337. <https://doi.org/10.1039/C8CC08992B>.
- 130** Lin, C., Zhang, H., Song, X. et al. (2020). 2D-organic framework confined metal single atoms with the loading reaching the theoretical limit. *Materials Horizons* 7 (10): 2726–2733. <https://doi.org/10.1039/D0MH01061H>.
- 131** Cheng, Y., Zhao, S., Li, H. et al. (2019). Unsaturated edge-anchored Ni single atoms on porous microwave exfoliated graphene oxide for electrochemical CO₂. *Applied Catalysis B: Environmental* 243: 294–303. <https://doi.org/10.1016/j.apcatb.2018.10.046>.
- 132** Zhao, S., Cheng, Y., Veder, J.-P. et al. (2018). One-pot pyrolysis method to fabricate carbon nanotube supported Ni single-atom catalysts with ultrahigh loading. *ACS Applied Energy Materials* 1 (10): 5286–5297. <https://doi.org/10.1021/acsaem.8b00903>.
- 133** Zhao, S., Wang, T., Zhou, G. et al. (2020). Controlled one-pot synthesis of nickel single atoms embedded in carbon nanotube and graphene supports with high loading. *ChemNanoMat* 6 (7): 1063–1074. <https://doi.org/10.1002/cnma.202000223>.
- 134** Guo, T., Tang, N., Lin, F. et al. (2020). High-loading single-atom copper catalyst supported on coordinatively unsaturated Al₂O₃ for selective synthesis of homoallylboronates. *ChemSusChem* 13 (12): 3115–3121. <https://doi.org/10.1002/cssc.202000536>.
- 135** Yang, P., Zuo, S., Zhang, F. et al. (2020). Carbon nitride-based single-atom Cu catalysts for highly efficient carboxylation of alkynes with atmospheric CO₂. *Industrial & Engineering Chemistry Research* 59 (16): 7327–7335. <https://doi.org/10.1021/acs.iecr.0c00547>.
- 136** Han, G., Zheng, Y., Zhang, X. et al. (2019). High loading single-atom Cu dispersed on graphene for efficient oxygen reduction reaction. *Nano Energy* 66: 104088. <https://doi.org/10.1016/j.nanoen.2019.104088>.
- 137** Li, J., Chen, S., Yang, N. et al. (2019). Ultrahigh-loading zinc single-atom catalyst for highly efficient oxygen reduction in both acidic and alkaline media. *Angewandte Chemie International Edition* 58 (21): 7035–7039. <https://doi.org/10.1002/anie.201902109>.
- 138** Yang, Q., Yang, C.-C., Lin, C.-H. et al. (2019). Metal-organic-framework-derived hollow N-doped porous carbon with ultrahigh concentrations of single Zn atoms for efficient carbon dioxide conversion. *Angewandte Chemie International Edition* 58 (11): 3511–3515. <https://doi.org/10.1002/anie.201813494>.
- 139** Tang, C., Jiao, Y., Shi, B. et al. (2020). Coordination tunes selectivity: two-electron oxygen reduction on high-loading molybdenum single-atom catalysts. *Angewandte Chemie International Edition* 59 (23): 9171–9176. <https://doi.org/10.1002/anie.202003842>.
- 140** Wang, L., Chen, M.-X., Yan, Q.-Q. et al. (2019). A sulfur-tethering synthesis strategy toward high-loading atomically dispersed noble metal catalysts. *Science Advances* 5 (10): eaax6322. <https://doi.org/10.1126/sciadv.aax6322>.
- 141** Ma, Y., Ren, Y., Zhou, Y. et al. (2020). High-density and thermally stable palladium single-atom catalysts for chemoselective hydrogenations. *Angewandte*

- Chemie International Edition* 59 (48): 21613–21619. <https://doi.org/10.1002/anie.202007707>.
- 142** Jiang, X.-H., Zhang, L.-S., Liu, H.-Y. et al. (2020). Silver single atom in carbon nitride catalyst for highly efficient photocatalytic hydrogen evolution. *Angewandte Chemie International Edition* 59 (51): 23112–23116. <https://doi.org/10.1002/anie.202011495>.
- 143** Chen, W., Pei, J., He, C.-T. et al. (2018). Single tungsten atoms supported on MOF-derived N-doped carbon for Robust electrochemical hydrogen evolution. *Advanced Materials* 30 (30): 1800396. <https://doi.org/10.1002/adma.201800396>.
- 144** Babucci, M., Sarac Oztuna, F.E., Debeve, L.M. et al. (2019). Atomically dispersed reduced graphene aerogel-supported iridium catalyst with an iridium loading of 14.8 wt %. *ACS Catalysis* 9 (11): 9905–9913. <https://doi.org/10.1021/acscatal.9b02231>.
- 145** Wang, Q., Huang, X., Zhao, Z.L. et al. (2020). Ultrahigh-loading of Ir single atoms on NiO matrix to dramatically enhance oxygen evolution reaction. *Journal of the American Chemical Society* 142 (16): 7425–7433. <https://doi.org/10.1021/jacs.9b12642>.
- 146** Li, H., Wang, L., Dai, Y. et al. (2018). Synergetic interaction between neighbouring platinum monomers in CO₂ hydrogenation. *Nature Nanotechnology* 13 (5): 411–417. <https://doi.org/10.1038/s41565-018-0089-z>.
- 147** Li, T., Liu, J., Song, Y. et al. (2018). Photochemical solid-phase synthesis of platinum single atoms on nitrogen-doped carbon with high loading as bifunctional catalysts for hydrogen evolution and oxygen reduction reactions. *ACS Catalysis* 8 (9): 8450–8458. <https://doi.org/10.1021/acscatal.8b02288>.
- 148** Zhu, Y., Cao, T., Cao, C. et al. (2018). One-pot pyrolysis to N-doped graphene with high-density Pt single atomic sites as heterogeneous catalyst for alkene hydrosilylation. *ACS Catalysis* 8 (11): 10004–10011. <https://doi.org/10.1021/acscatal.8b02624>.
- 149** Kunwar, D., Zhou, S., DeLaRiva, A. et al. (2019). Stabilizing high metal loadings of thermally stable platinum single atoms on an industrial catalyst support. *ACS Catalysis* 9 (5): 3978–3990. <https://doi.org/10.1021/acscatal.8b04885>.
- 150** Cao, S., Zhao, Y., Lee, S. et al. (2020). High-loading single Pt atom sites [Pt-O(OH)_x] catalyze the CO PROX reaction with high activity and selectivity at mild conditions. *Science Advances* 6 (25): eaba3809. <https://doi.org/10.1126/sciadv.aba3809>.
- 151** Liu, K., Tang, Y., Yu, Z. et al. (2020). High-loading and thermally stable Pt₁/MgAl_{1.2}Fe_{0.8}O₄ single-atom catalysts for high-temperature applications. *Science China Materials* 63 (6): 949–958. <https://doi.org/10.1007/s40843-020-1267-2>.
- 152** Zuo, Q., Liu, T., Chen, C. et al. (2019). Ultrathin metal–organic framework nanosheets with ultrahigh loading of single Pt atoms for efficient visible-light-driven photocatalytic H₂ evolution. *Angewandte Chemie International Edition* 58 (30): 10198–10203. <https://doi.org/10.1002/anie.201904058>.

- 153 Wang, Z., Gu, L., Song, L. et al. (2018). Facile one-pot synthesis of MOF supported gold pseudo-single-atom catalysts for hydrogenation reactions. *Materials Chemistry Frontiers* 2 (5): 1024–1030. <https://doi.org/10.1039/C8QM00081F>.
- 154 Tan, K., Dixit, M., Dean, J. et al. (2019). Predicting metal–support interactions in oxide-supported single-atom catalysts. *Industrial & Engineering Chemistry Research* 58 (44): 20236–20246. <https://doi.org/10.1021/acs.iecr.9b04068>.
- 155 Davies, P.R. and Morgan, D.J. (2020). Practical guide for X-ray photoelectron spectroscopy: applications to the study of catalysts. *Journal of Vacuum Science & Technology A* 38 (3): 033204. <https://doi.org/10.1116/1.5140747>.
- 156 Hulva, J., Meier, M., Bliem, R. et al. (2021). Unraveling CO adsorption on model single-atom catalysts. *Science* 371 (6527): 375–379. <https://doi.org/10.1126/science.abe5757>.
- 157 O’Shea, J.N., Schnadt, J., Andersson, S. et al. (2000). X-ray photoelectron spectroscopy of low surface concentration mass-selected Ag clusters. *The Journal of Chemical Physics* 113 (20): 9233–9238. <https://doi.org/10.1063/1.1319700>.
- 158 Vedrine, J.C., Dufaux, M., Naccache, C. et al. (1978). X-ray photoelectron spectroscopy study of Pd and Pt ions in type Y-zeolite. Electron transfer between metal aggregates and the support as evidenced by X-ray photoelectron spectroscopy and electron spin resonance. *Journal of the Chemical Society, Faraday Transactions 1: Physical Chemistry in Condensed Phases* 74: 440–449. <https://doi.org/10.1039/F19787400440>.
- 159 Stakheev, A.Y. and Sachtler, W.M.H. (1991). Determination by X-ray photoelectron spectroscopy of the electronic state of Pd clusters in Y zeolite. *Journal of the Chemical Society, Faraday Transactions* 87 (22): 3703–3708. <https://doi.org/10.1039/FT9918703703>.
- 160 Bastl, Z. (1986). X-ray photoelectron spectroscopy of supported metal particles. *Vacuum* 36 (7): 447–448. [https://doi.org/10.1016/0042-207X\(86\)90225-3](https://doi.org/10.1016/0042-207X(86)90225-3).
- 161 Feng, K., Zhang, H., Gao, J. et al. (2020). Single atoms or not? The limitation of EXAFS. *Applied Physics Letters* 116 (19): 191903. <https://doi.org/10.1063/5.0008748>.
- 162 Petek, U., Ruiz-Zepeda, F., Bele, M. et al. (2019). Nanoparticles and single atoms in commercial carbon-supported platinum-group metal catalysts. *Catalysts* 9 (2): 134.
- 163 Kuai, L., Chen, Z., Liu, S. et al. (2020). Titania supported synergistic palladium single atoms and nanoparticles for room temperature ketone and aldehydes hydrogenation. *Nature Communications* 11 (1): 48. <https://doi.org/10.1038/s41467-019-13941-5>.
- 164 Ma, Y., Yang, T., Zou, H. et al. (2020). Synergizing Mo single atoms and Mo₂C nanoparticles on CNTs synchronizes selectivity and activity of electrocatalytic N₂ reduction to ammonia. *Advanced Materials* 32 (33): 2002177. <https://doi.org/10.1002/adma.202002177>.
- 165 Fu, Y., Xu, D., Wang, Y. et al. (2020). Single atoms anchored on cobalt-based catalysts derived from hydrogels containing phthalocyanine toward the oxygen reduction reaction. *ACS Sustainable Chemistry & Engineering* 8 (22): 8338–8347. <https://doi.org/10.1021/acssuschemeng.0c02158>.

- 166 Tiwari, J.N., Dang, N.K., Park, H.J. et al. (2020). Remarkably enhanced catalytic activity by the synergistic effect of palladium single atoms and palladium-cobalt phosphide nanoparticles. *Nano Energy* 78: 105166. <https://doi.org/10.1016/j.nanoen.2020.105166>.
- 167 Peng, J., Chen, Y., Wang, K. et al. (2020). High-performance Ru-based electrocatalyst composed of Ru nanoparticles and Ru single atoms for hydrogen evolution reaction in alkaline solution. *International Journal of Hydrogen Energy* 45 (38): 18840–18849. <https://doi.org/10.1016/j.ijhydene.2020.05.064>.
- 168 Yuan, B., Yao, Z., Qiu, C. et al. (2020). Synergistic effect of size-dependent PtZn nanoparticles and zinc single-atom sites for electrochemical ozone production in neutral media. *Journal of Energy Chemistry* 51: 312–322. <https://doi.org/10.1016/j.jechem.2020.03.066>.
- 169 Wang, L., Guan, E., Zhang, J. et al. (2018). Single-site catalyst promoters accelerate metal-catalyzed nitroarene hydrogenation. *Nature Communications* 9 (1): 1362. <https://doi.org/10.1038/s41467-018-03810-y>.
- 170 Liu, D., He, Q., Ding, S. et al. (2020). Structural regulation and support coupling effect of single-atom catalysts for heterogeneous catalysis. *Advanced Energy Materials* 10 (32): 2001482. <https://doi.org/10.1002/aenm.202001482>.
- 171 Lai, W.-H., Miao, Z., Wang, Y.-X. et al. (2019). Atomic-local environments of single-atom catalysts: synthesis, electronic structure, and activity. *Advanced Energy Materials* 9 (43): 1900722. <https://doi.org/10.1002/aenm.201900722>.
- 172 Crabtree, R.H. (1983). Cationic rhodium and iridium complexes in catalysis. In: *Homogeneous Catalysis with Metal Phosphine Complexes* (ed. L.H. Pignolet), 297–316. Boston, MA: Springer US.
- 173 Tosoni, S. and Pacchioni, G. (2020). Bonding properties of isolated metal atoms on two-dimensional oxides. *The Journal of Physical Chemistry C* 124 (38): 20960–20973. <https://doi.org/10.1021/acs.jpcc.0c05958>.
- 174 Tang, Y., Zhao, S., Long, B. et al. (2016). On the nature of support effects of metal dioxides MO₂ (M = Ti, Zr, Hf, Ce, Th) in single-atom gold catalysts: importance of quantum primogenic effect. *The Journal of Physical Chemistry C* 120 (31): 17514–17526. <https://doi.org/10.1021/acs.jpcc.6b05338>.
- 175 Camellone, M.F. and Fabris, S. (2009). Reaction mechanisms for the CO oxidation on Au/CeO₂ catalysts: activity of substitutional Au³⁺/Au⁺ cations and deactivation of supported Au⁺ adatoms. *Journal of the American Chemical Society* 131 (30): 10473–10483. <https://doi.org/10.1021/ja902109k>.
- 176 Tang, Y., Wang, Y.-G., and Li, J. (2017). Theoretical investigations of Pt₁@CeO₂ single-atom catalyst for CO oxidation. *The Journal of Physical Chemistry C* 121 (21): 11281–11289. <https://doi.org/10.1021/acs.jpcc.7b00313>.
- 177 Parkinson, G.S. (2019). Single-atom catalysis: how structure influences catalytic performance. *Catalysis Letters* 149 (5): 1137–1146. <https://doi.org/10.1007/s10562-019-02709-7>.
- 178 Fu, Z., Yang, B., and Wu, R. (2020). Understanding the activity of single-atom catalysis from frontier orbitals. *Physical Review Letters* 125 (15): 156001. <https://doi.org/10.1103/PhysRevLett.125.156001>.

- 179** Chen, P., Zhou, T., Xing, L. et al. (2017). Atomically dispersed iron–nitrogen species as electrocatalysts for bifunctional oxygen evolution and reduction reactions. *Angewandte Chemie International Edition* 56 (2): 610–614. <https://doi.org/10.1002/anie.201610119>.
- 180** Lou, Y., Zheng, Y., Li, X. et al. (2019). Pocketlike active site of Rh₁/MoS₂ single-atom catalyst for selective crotonaldehyde hydrogenation. *Journal of the American Chemical Society* 141 (49): 19289–19295. <https://doi.org/10.1021/jacs.9b06628>.
- 181** Li, Z., Wang, D., Wu, Y. et al. (2018). Recent advances in the precise control of isolated single-site catalysts by chemical methods. *National Science Review* 5 (5): 673–689. <https://doi.org/10.1093/nsr/nwy056>.
- 182** Qi, K., Chhowalla, M., and Voiry, D. (2020). Single atom is not alone: metal–support interactions in single-atom catalysis. *Materials Today* 40: 173–192. <https://doi.org/10.1016/j.mattod.2020.07.002>.
- 183** Costa-Amaral, R., Forhat, A., Caturello, N.A.M.S. et al. (2020). Unveiling the adsorption properties of 3d, 4d, and 5d metal adatoms on the MoS₂ monolayer: a DFT-D3 investigation. *Surface Science* 701: 121700. <https://doi.org/10.1016/j.susc.2020.121700>.
- 184** Chen, Z., Zhao, J., Cabrera, C.R. et al. (2019). Computational screening of efficient single-atom catalysts based on graphitic carbon nitride (g-C₃N₄) for nitrogen electroreduction. *Small Methods* 3 (6): 1800368. <https://doi.org/10.1002/smtd.201800368>.
- 185** Nagashima, H., Nakaoka, A., Saito, Y. et al. (1992). C₆₀Pd: the first organometallic polymer of buckminsterfullerene. *Journal of the Chemical Society, Chemical Communications* 4: 377–379. <https://doi.org/10.1039/C39920000377>.
- 186** Lavrentiev, V., Abe, H., Naramoto, H. et al. (2006). Polymeric chains in C₆₀ and Co mixture. *Chemical Physics Letters* 424 (1): 101–104. <https://doi.org/10.1016/j.cplett.2006.04.046>.
- 187** Leng, F., Gerber, I.C., Lecante, P. et al. (2016). Synthesis and structure of ruthenium-fullerides. *RSC Advances* 6 (73): 69135–69148. <https://doi.org/10.1039/C6RA12023G>.
- 188** Hülsey, M.J., Zhang, J., and Yan, N. (2018). Harnessing the wisdom in colloidal chemistry to make stable single-atom catalysts. *Advanced Materials* 30 (47): 1802304. <https://doi.org/10.1002/adma.201802304>.
- 189** Liu, J.-C., Tang, Y., Wang, Y.-G. et al. (2018). Theoretical understanding of the stability of single-atom catalysts. *National Science Review* 5 (5): 638–641. <https://doi.org/10.1093/nsr/nwy094>.
- 190** Jones, J., Xiong, H., DeLaRiva, A.T. et al. (2016). Thermally stable single-atom platinum-on-ceria catalysts via atom trapping. *Science* 353 (6295): 150–154. <https://doi.org/10.1126/science.aaf8800>.
- 191** Qiao, B., Liang, J.-X., Wang, A. et al. (2015). Ultrastable single-atom gold catalysts with strong covalent metal-support interaction (CMSI). *Nano Research* 8 (9): 2913–2924. <https://doi.org/10.1007/s12274-015-0796-9>.

- 192** Wei, S., Li, A., Liu, J.-C. et al. (2018). Direct observation of noble metal nanoparticles transforming to thermally stable single atoms. *Nature Nanotechnology* 13 (9): 856–861. <https://doi.org/10.1038/s41565-018-0197-9>.
- 193** Lang, R., Xi, W., Liu, J.-C. et al. (2019). Non defect-stabilized thermally stable single-atom catalyst. *Nature Communications* 10 (1): 234. <https://doi.org/10.1038/s41467-018-08136-3>.
- 194** O'Connor, N.J., Jonayat, A.S.M., Janik, M.J. et al. (2018). Interaction trends between single metal atoms and oxide supports identified with density functional theory and statistical learning. *Nature Catalysis* 1 (7): 531–539. <https://doi.org/10.1038/s41929-018-0094-5>.
- 195** Liu, L. and Corma, A. (2020). Evolution of isolated atoms and clusters in catalysis. *Trends in Chemistry* 2 (4): 383–400. <https://doi.org/10.1016/j.trechm.2020.02.003>.
- 196** Campbell, C.T. (2013). The energetics of supported metal nanoparticles: relationships to sintering rates and catalytic activity. *Accounts of Chemical Research* 46 (8): 1712–1719. <https://doi.org/10.1021/ar3003514>.
- 197** Rickard, J.M., Genovese, L., Moata, A. et al. (1990). Redispersed of platinum on Pt/Al₂O₃ model catalyst in oxygen studied by transmission electron microscopy. *Journal of Catalysis* 121 (1): 141–152. [https://doi.org/10.1016/0021-9517\(90\)90224-8](https://doi.org/10.1016/0021-9517(90)90224-8).
- 198** Lai, X. and Goodman, D.W. (2000). Structure–reactivity correlations for oxide-supported metal catalysts: new perspectives from STM. *Journal of Molecular Catalysis A: Chemical* 162 (1): 33–50. [https://doi.org/10.1016/S1381-1169\(00\)00320-4](https://doi.org/10.1016/S1381-1169(00)00320-4).
- 199** Zhou, J., Kang, Y.C., and Chen, D.A. (2003). Oxygen-induced dissociation of Cu islands supported on TiO₂(110). *The Journal of Physical Chemistry B* 107 (28): 6664–6667. <https://doi.org/10.1021/jp0301251>.
- 200** Zhou, J., Kang, Y.C., Ma, S. et al. (2004). Adsorbate-induced dissociation of metal clusters: TiO₂(110)-supported Cu and Ni clusters exposed to oxygen gas. *Surface Science* 562 (1): 113–127. <https://doi.org/10.1016/j.susc.2004.05.094>.
- 201** Simonsen, S.B., Chorkendorff, I., Dahl, S. et al. (2010). Direct observations of oxygen-induced platinum nanoparticle ripening studied by in situ TEM. *Journal of the American Chemical Society* 132 (23): 7968–7975. <https://doi.org/10.1021/ja910094r>.
- 202** Moliner, M., Gabay, J., Kliewer, C. et al. (2018). Trapping of metal atoms and metal clusters by chabazite under severe redox stress. *ACS Catalysis* 8 (10): 9520–9528. <https://doi.org/10.1021/acscatal.8b01717>.
- 203** Moliner, M., Gabay, J.E., Kliewer, C.E. et al. (2016). Reversible transformation of Pt nanoparticles into single atoms inside high-silica chabazite zeolite. *Journal of the American Chemical Society* 138 (48): 15743–15750. <https://doi.org/10.1021/jacs.6b10169>.
- 204** Feng, S., Lin, X., Song, X. et al. (2020). The role of H₂ on the stability of the single-metal-site Ir1/AC catalyst for heterogeneous methanol carbonylation. *Journal of Catalysis* 381: 193–203. <https://doi.org/10.1016/j.jcat.2019.10.032>.

- 205 Nelson, N.C., Chen, L., Meira, D. et al. (2020). In situ dispersion of palladium on TiO₂ during reverse water–gas shift reaction: formation of atomically dispersed palladium. *Angewandte Chemie International Edition* 59 (40): 17657–17663. <https://doi.org/10.1002/anie.202007576>.
- 206 Ding, S., Guo, Y., Hülsey, M.J. et al. (2019). Electrostatic stabilization of single-atom catalysts by ionic liquids. *Chem* 5 (12): 3207–3219. <https://doi.org/10.1016/j.chempr.2019.10.007>.
- 207 Wei, H., Huang, K., Wang, D. et al. (2017). Iced photochemical reduction to synthesize atomically dispersed metals by suppressing nanocrystal growth. *Nature Communications* 8 (1): 1490. <https://doi.org/10.1038/s41467-017-01521-4>.
- 208 Wang, Y., Song, E., Qiu, W. et al. (2019). Recent progress in theoretical and computational investigations of structural stability and activity of single-atom electrocatalysts. *Progress in Natural Science: Materials International* 29 (3): 256–264. <https://doi.org/10.1016/j.pnsc.2019.04.004>.
- 209 Li, J., Guan, Q., Wu, H. et al. (2019). Highly active and stable metal single-atom catalysts achieved by strong electronic metal–support interactions. *Journal of the American Chemical Society* 141 (37): 14515–14519. <https://doi.org/10.1021/jacs.9b06482>.
- 210 Su, Y.-Q., Zhang, L., Wang, Y. et al. (2020). Stability of heterogeneous single-atom catalysts: a scaling law mapping thermodynamics to kinetics. *npj Computational Materials* 6 (1): 144. <https://doi.org/10.1038/s41524-020-00411-6>.
- 211 Lu, Z., Yadav, S., and Singh, C.V. (2020). Predicting aggregation energy for single atom bimetallic catalysts on clean and O* adsorbed surfaces through machine learning models. *Catalysis Science & Technology* 10 (1): 86–98. <https://doi.org/10.1039/C9CY02070E>.
- 212 Lin, S., Xu, H., Wang, Y. et al. (2020). Directly predicting limiting potentials from easily obtainable physical properties of graphene-supported single-atom electrocatalysts by machine learning. *Journal of Materials Chemistry A* 8 (11): 5663–5670. <https://doi.org/10.1039/C9TA13404B>.
- 213 Dasgupta, A., Gao, Y., Broderick, S.R. et al. (2020). Machine learning-aided identification of single atom alloy catalysts. *The Journal of Physical Chemistry C* 124 (26): 14158–14166. <https://doi.org/10.1021/acs.jpcc.0c01492>.
- 214 Wang, Y., Su, Y.-Q., Hensen, E.J.M. et al. (2020). Finite-temperature structures of supported subnanometer catalysts inferred via statistical learning and genetic algorithm-based optimization. *ACS Nano* 14 (10): 13995–14007. <https://doi.org/10.1021/acsnano.0c06472>.
- 215 Boyes, E.D., LaGrow, A.P., Ward, M.R. et al. (2020). Single atom dynamics in chemical reactions. *Accounts of Chemical Research* 53 (2): 390–399. <https://doi.org/10.1021/acs.accounts.9b00500>.
- 216 Li, X., Yang, X., Zhang, J. et al. (2019). In situ/operando techniques for characterization of single-atom catalysts. *ACS Catalysis* 9 (3): 2521–2531. <https://doi.org/10.1021/acscatal.8b04937>.
- 217 Xi, W., Wang, K., Shen, Y. et al. (2020). Dynamic co-catalysis of Au single atoms and nanoporous Au for methane pyrolysis. *Nature Communications* 11 (1): 1919. <https://doi.org/10.1038/s41467-020-15806-8>.

- 218 Gaikwad, A.V., Holuigue, A., Thathagar, M.B. et al. (2007). Ion- and atom-leaching mechanisms from palladium nanoparticles in cross-coupling reactions. *Chemistry A European Journal* 13 (24): 6908–6913. <https://doi.org/10.1002/chem.200700105>.
- 219 Trzeciak, A.M. and Augustyniak, A.W. (2019). The role of palladium nanoparticles in catalytic C–C cross-coupling reactions. *Coordination Chemistry Reviews* 384: 1–20. <https://doi.org/10.1016/j.ccr.2019.01.008>.
- 220 Dessal, C., Len, T., Morfin, F. et al. (2019). Dynamics of single Pt atoms on alumina during CO oxidation monitored by operando X-ray and infrared spectroscopies. *ACS Catalysis* 9 (6): 5752–5759. <https://doi.org/10.1021/acscatal.9b00903>.
- 221 Karapinar, D., Huan, N.T., Ranjbar, S.N. et al. (2019). Electroreduction of CO₂ on single-site copper-nitrogen-doped carbon material: selective formation of ethanol and reversible restructuring of the metal sites. *Angewandte Chemie International Edition* 58 (42): 15098–15103. <https://doi.org/10.1002/anie.201907994>.
- 222 Daelman, N., Capdevila-Cortada, M., and López, N. (2019). Dynamic charge and oxidation state of Pt/CeO₂ single-atom catalysts. *Nature Materials* 18 (11): 1215–1221. <https://doi.org/10.1038/s41563-019-0444-y>.
- 223 Butin, K.P., Beloglazkina, E.K., and Zyk, N.V. (2005). Metal complexes with non-innocent ligands. *Russian Chemical Reviews* 74 (6): 531–553. <https://doi.org/10.1070/rc2005v074n06abeh000977>.
- 224 Ganguly, S. and Ghosh, A. (2019). Seven clues to ligand noninnocence: the metallocorrole paradigm. *Accounts of Chemical Research* 52 (7): 2003–2014. <https://doi.org/10.1021/acs.accounts.9b00115>.
- 225 Lyaskovskyy, V. and de Bruin, B. (2012). Redox non-innocent ligands: versatile new tools to control catalytic reactions. *ACS Catalysis* 2 (2): 270–279. <https://doi.org/10.1021/cs200660v>.
- 226 Kaim, W. and Schwederski, B. (2010). Non-innocent ligands in bioinorganic chemistry—an overview. *Coordination Chemistry Reviews* 254 (13): 1580–1588. <https://doi.org/10.1016/j.ccr.2010.01.009>.
- 227 DeRita, L., Resasco, J., Dai, S. et al. (2019). Structural evolution of atomically dispersed Pt catalysts dictates reactivity. *Nature Materials* 18 (7): 746–751. <https://doi.org/10.1038/s41563-019-0349-9>.
- 228 Paolucci, C., Khurana, I., Parekh, A.A. et al. (2017). Dynamic multinuclear sites formed by mobilized copper ions in NO_x selective catalytic reduction. *Science* 357 (6354): 898–903. <https://doi.org/10.1126/science.aan5630>.
- 229 Zhang, L., Long, R., Zhang, Y. et al. (2020). Direct observation of dynamic bond evolution in single-atom Pt/C₃N₄ catalysts. *Angewandte Chemie International Edition* 59 (15): 6224–6229. <https://doi.org/10.1002/anie.201915774>.
- 230 Qiu, S., Li, Q., Xu, Y. et al. (2020). Learning from nature: understanding hydrogenase enzyme using computational approach. *WIREs Computational Molecular Science* 10 (1): e1422. <https://doi.org/10.1002/wcms.1422>.

- 231** Chowdhury, R. and Maranas, C.D. (2020). From directed evolution to computational enzyme engineering—a review. *AIChE Journal* 66 (3): e16847. <https://doi.org/10.1002/aic.16847>.
- 232** Fu, L., Tang, Y., and Lin, Y. (2020). Advances in synchrotron radiation-based X-ray absorption spectroscopy to characterize the fine atomic structure of single-atom nanozymes. *Chemistry - An Asian Journal* 15 (14): 2110–2116. <https://doi.org/10.1002/asia.202000560>.
- 233** Boyes, E.D., LaGrow, A.P., Ward, M.R. et al. (2020). Visualizing single atom dynamics in heterogeneous catalysis using analytical *in situ* environmental scanning transmission electron microscopy. *Philosophical Transactions of the Royal Society A: Mathematical, Physical and Engineering Sciences* 378 (2186): 20190605. <https://doi.org/10.1098/rsta.2019.0605>.
- 234** Li, L., Chang, X., Lin, X. et al. (2020). Theoretical insights into single-atom catalysts. *Chemical Society Reviews* 49: 8156–8178. <https://doi.org/10.1039/D0CS00795A>.

